UNIVERSIDADE ESTADUAL PAULISTA
"JÚLIO DE MESQUITA FILHO"
Faculdade de Engenharia de São João da Boa Vista

Nícholas Fonseca Martins

Design and fabrication of helical antennas with non-uniform cross-section wire via metal additive manufacturing

São João da Boa Vista

2024

Nícholas Fonseca Martins

Design and fabrication of helical antennas with non-uniform cross-section wire via metal additive manufacturing

Dissertation presented to the School of Engineering of São Paulo State University, São João da Boa Vista Campus, as a partial requirement for the Master's degree in Electrical Engineering within the Graduate Program in Electrical Engineering.

Concentration Area: Electronic Systems

Supervisor: Prof. Dr. Rafael Abrantes Penchel

Co-supervisor: Prof. Dr. Denilson Paulo S. dos Santos

São João da Boa Vista

2024

M386d

Martins, Nícholas Fonseca
Design and fabrication of helical antennas with non-uniform cross-section wire via metal additive manufacturing / Nícholas Fonseca Martins. -- São João da Boa Vista, 2024
52 p. : il., tabs.

Dissertação (mestrado) - Universidade Estadual Paulista (UNESP), Faculdade de Engenharia, São João da Boa Vista
Orientador: Rafael Abrantes Penchel
Coorientador: Denilson Paulo S. dos Santos

1. Antennas (Electronics). 2. Microwave antennas. 3. Microwave communication systems. 4. Microwave communication systems. I. Título.

Sistema de geração automática de fichas catalográficas da Unesp. Biblioteca da Universidade Estadual Paulista (UNESP), Faculdade de Engenharia, São João da Boa Vista. Dados fornecidos pelo autor(a).

Essa ficha não pode ser modificada.

IMPACTO POTENCIAL DESTA PESQUISA

Esta pesquisa apresenta uma nova formulação matemática para antenas helicoidais, variando diâmetro, espaçamento e seção transversal do fio. Com técnicas de otimização, essas antenas são mais eficientes e contribuem para a inovação tecnológica e avanço das comunicações, beneficiando a sociedade com soluções avançadas e resilientes.

POTENTIAL IMPACT OF THIS RESEARCH

This research presents a new mathematical formulation for helical antennas, varying the diameter, spacing and cross-section of the wire. With optimization techniques, these antennas are more efficient and contribute to technological innovation and the advancement of communications, benefiting society with advanced and resilient solutions.

UNIVERSIDADE ESTADUAL PAULISTA

Câmpus de São João da Boa Vista

CERTIFICADO DE APROVAÇÃO

TÍTULO DA DISSERTAÇÃO: Design and fabrication of helical antennas with non-uniform cross-section wire via metal additive manufacturing

AUTOR: NÍCHOLAS FONSECA MARTINS
ORIENTADOR: RAFAEL ABRANTES PENCHEL
COORIENTADOR: DENILSON PAULO SOUZA DOS SANTOS

Aprovado como parte das exigências para obtenção do Título de Mestre em Engenharia Elétrica, área: Sistemas Eletrônicos pela Comissão Examinadora:

Prof. Dr. RAFAEL ABRANTES PENCHEL (Participaçao Virtual)
Departamento de Engenharia Eletronica e de Telecomunicacoes / Faculdade de Engenharia de Sao Joao da Boa Vista UNESP

Prof. Dr. IVAN ARITZ ALDAYA GARDE (Participaçao Virtual)
Departamento de Engenharia Eletronica e de Telecomunicacoes / Faculdade de Engenharia de Sao Joao da Boa Vista UNESP

Prof. Dr. RENAN ALVES DOS SANTOS (Participaçao Virtual)
Faculdade de Engenharia Elétrica / Universidade Federal de Uberlândia

São João da Boa Vista, 22 de março de 2024

Renan Roberto Rubim
Supervisor Técnico Substituto
de Seção Técnica de Graduação e Pós-Graduação

To the divine guidance of God and the ongoing scientific development of our country.

Acknowledgements

I would like to sincerely thank everyone who, in some way, contributed to the completion of this work. First of all, I would like to express my deepest gratitude to my dear parents, Antônio and Vani. Their unconditional support and love were true driving forces that motivated me to keep going, even in the most challenging times.

I extend my sincere thanks to the dedicated professors who generously shared their knowledge throughout my postgraduate studies. Every class, discussion and piece of guidance played a key role in developing my critical thinking and enhancing my academic training.

To my advisory team, composed of Professor Rafael Abrantes Penchel and advisor Professor Denilson Paulo S. dos Santos, I dedicate my deepest gratitude. Thank you for guiding me with wisdom, patience, and expertise throughout this academic journey. Their valuable contributions have been essential in deepening my understanding of the subject, shaping not only the work, but also my professional and academic growth.

I now especially want to thank my esteemed advisor, Professor Rafael. His guidance was a shining beacon that illuminated my academic path. His passion for research, patience, tireless commitment, and ability to instigate critical thinking were key elements in the success of this work. Without his dedication, this project would not have reached the heights it did. Your influence goes beyond the academic aspects and is reflected in my formation as a professional and as an individual.

I also want to thank you for the financial support of under grant #409146/2021-8, The Brazilian agencies National Council for Scientific and Technological Development (CNPq), under grant #2020/09889-4, São Paulo Research Foundation (FAPESP), and under grant #0527/18, Financier of Studies and Projects (FINEP),

To Professor Dr. Guilherme Simon da Rosa, whose tireless support was fundamental to the success of this project. His expertise and dedication in carrying out the helical antenna tests in the anechoic chamber at PUC-RJ were crucial to the progress of this research. I am deeply grateful for your guidance, patience and commitment, which made it possible to achieve our goals. Your contribution was indispensable and will forever be valued.

To God for the grace and wisdom granted to me throughout this journey. I recognize His divine guidance as indispensable for overcoming seemingly impossible challenges. I dedicate this work to Him, recognizing His hand present at all times.

Finally, I would like to thank everyone who has contributed in some way to this achievement. This work is the result of a collective effort that reflects the support, collaboration, and inspiration of many. To everyone who has been by my side on this journey, my deepest thanks.

"All the mathematical sciences are founded on the relations between physical laws and laws of numbers."

(James Clerk Maxwell, 1856)

Abstract

This dissertation presents a study on helical antennas, introducing a new mathematical formulation for representing the helix, in which the diameter, spacing, and cross-section of the metal wire are non-uniform. It is demonstrated how these modifications, combined with optimization techniques, can be used to improve the electromagnetic performance of designed antennas. Precisely defining the transition region between the helix and the central feeding point, a thicker wire was strategically employed at the base to enhance both the antenna's operational bandwidth and mechanical strength, eliminating the need for additional support structures. The wire diameter was linearly reduced towards the top of the helix to improve radiation characteristics. To address the manufacturing challenges presented by the complex geometries of non-uniform helical antennas, the additive metal manufacturing process was employed. Maraging steel was chosen for its ability to withstand severe environmental conditions and temperature fluctuations without experiencing significant deformations, distinguishing it from polymer alternatives. The proposed formulation was explored using three models tailored for the X-band (8 GHz to 12 GHz): Model I) A standard helical antenna featuring uniform diameter and helix spacing; Model II) a helical antenna with non-uniform diameter and helix spacing; and Model III) a helical antenna with non-uniform diameter, cross-section, and helix spacing. The findings illustrate that the helical antenna utilizing a tapered cross-section wire (thicker at the base and thinner at the tip) exhibits significantly superior performance compared to the control models. Specifically, we present an eight-turn helical antenna that attained a measured reflection coefficient below -10dB and an axial ratio of less than 1dB across the X-band, with a peak realized gain in right-hand circular polarization (RHCP) of 10.8dBic.

Keywords: Circular polarization, helical antenna; non-uniform pitch angle; axial mode; X band; additive manufacturing.

Resumo

Esta dissertação apresenta um estudo sobre antenas helicoidais, introduzindo uma nova formulação matemática para a representação da hélice, no qual o diâmetro, espaçamento e seção transversal do fio metálico não são uniformes. É demonstrado como essas modificações, combinadas à técnicas de otimização, pode ser utilizadas para melhorar o desempenho eletromagnético das antenas projetadas. Definindo de forma precisa a região de transição entre a hélice e o ponto de alimentação central, um fio mais grosso foi estrategicamente empregado na base para aprimorar tanto a largura de banda operacional da antena quanto a resistência mecânica, eliminando a necessidade de estruturas de suporte adicionais. O diâmetro do fio foi linearmente reduzido até o topo da hélice para melhorar as características de radiação. Para lidar com os desafios de fabricação apresentados pelas geometrias complexas das antenas helicoidais não uniformes foi utilizado o processo de manufatura aditiva de metais. Foi escolhido aço Maraging por apresentar a suporte condições ambientais severas e flutuações de temperatura sem experimentar deformações significativas, distinguindo-a das alternativas de polímeros. A formulação proposta foi explorada usando três modelos projetados para a banda X (8 GHz a 12 GHz): Modelo I) Uma antena helicoidal padrão apresentando diâmetro e espaçamento das hélices uniformes; Modelo II) uma antena helicoidal com diâmetro e espaçamento das hélices não uniformes; e Modelo III) uma antena helicoidal com diâmetro, seção transversal e espaçamento das hélices não uniformes. Os resultados mostram que a antena helicoidal utilizando um fio de seção transversal cônica (mais grosso na base e mais fino na ponta) exibe desempenho significativamente superior em comparação com os modelos de controle. Especificamente, apresentamos uma antena helicoidal de oito voltas que alcançou um coeficiente de reflexão medido abaixo de -10 dB e uma razão axial de menos de 1 dB em toda a banda X, com um ganho máximo realizado em polarização circular à direita (RHCP) de 10.8 dBic.

Palavras-chave: Polarização circular; antena helicoidal; ângulo de pitch não uniforme; modo axial; banda X; manufatura aditiva.

List of Figures

List of Tables

List of abbreviations and acronyms

AI	Artificial Intelligence
AM	Additive Manufacturing
AR	Axial Ratio
CAD	Computer-Aided Design
CNPQ	Brazilian agencies National Council for Scientific and Technological Development
CubeSat	Cube & Satellite
CNC	Computer Numeric Control
CPRR	Cross-Polarization Rejection Rate
dB	Decibels
dBi	Decibels relative to isotropic radiator
dBic	Decibels relative to isotropic radiator circularly polarized
FAPESP	São Paulo Research Foundation
FINEP	Financier of Studies and Projects
FEM	Finite Element Method
GNSS	Global Navigation Satellite System
HFSS	High Frequency Structure Simulator
IoT	Internet of Things
MAM	Metal Additive Manufacturing
PSO	Particle Swarm Optimization
LHCP	Left-Handed Circular Polarization
RHCP	Right-Handed Circular Polarization.
SLA	Stereolithography
SLS	Selective Laser Sintering

List of symbols

α_n	Pitch angle
α_z	Coefficient used to Control the Axial Profile of The Helix
α_ϕ	Coefficient used to Control the Radial Profile of the Helix
ℓ	Length of the Wire
λ_0	Central Wavelength of the Operating Band
D_n	Helices Diameter
d_e	Hole in the Reflector Plane
d_i	Diameter of the Central Pin
d_L	Diameter of the Helix Initial Section
d_N	Diameter of the Wire's Cross-Section
f_0	Central frequency
g_D	Diameter of Reflecting Ground Plane
g_L	Distance between the ground plane and the first helix
H	Helix Heights
L	Length of Helix
L_n	Length of each Helix
N	Number of Helices
R	Helix Radius
S	Spacing between Helices
S_n	Distance between the Helices

Contents

1 Introduction

1.1 Helical Antennas

The need for internet connectivity from any location at all times, the demand for wireless data transmission services at gigabit-per-second transfer rates, and the anticipation of widespread machine-to-machine communication (i.e., the popularization of the Internet of Things - IoT) have imposed challenging requirements on radiating systems in terms of dimensions, bandwidth behavior, and gain. As a consequence, the complexity of antenna geometry has increased, necessitating the use of new manufacturing techniques that are more efficient and environmentally sustainable.In response to these challenges, there is a growing demand for antennas with advanced features that can meet the evolving requirements of modern communication systems. This includes the development of compact antennas with broad bandwidth, high gain, and adaptability to various communication scenarios. Additionally, the environmental impact of manufacturing processes has become a significant consideration, driving the need for more eco-friendly and resource-efficient fabrication techniques. Helical antennas offer a unique combination of characteristics that make them indispensable in meeting these challenges.Their directivity pattern, wide bandwidth, and compact form factor address the need for efficient utilization of limited space while ensuring reliable communication over a broad frequency range. In this context, helical antennas emerge as a vital component in the arsenal of solutions aimed at shaping the future of wireless communication. With their ability to deliver high performance in diverse applications while promoting eco-friendly fabrication techniques, helical antennas seamlessly integrate into the vision of next-generation communication networks, propelling us toward a more connected, efficient, and sustainable digital future.

As we strive to meet the demands of global internet access, high-data transfer rates, and the proliferation of IoT, the evolution of antenna design and manufacturing plays a crucial role in shaping the future of wireless communication systems. Helical antennas have been fundamental in a wide kind of telecommunications applications due to their versatility and distinctive circularly polarized radiation properties. Particulary, in the X-band (8 to 12 GHz), helical antennas are extensively used in mobile satellite communications. They prove to be effective within this frequency range, contributing to reliable and efficient communication links for mobile satellite services (KRAUS, 1988), (BALANIS, 2016).

A helical antenna is characterized by its spiral or helix-shaped structure (KRAUS, 1988).The specific configuration allows the helical antenna to exhibit desirable electromagnetic characteristics in various wireless communication applications. Examples of applications for helical antennas include satellite communication, vehicle tracking systems, emergency communication in remote areas, and data transmission in densely populated urban environments. The helical antenna is composed of one or more metal conductors spiraled around a central axis. The number of turns in the helix, the spacing between the turns, and the antenna's diameter affect it is impedance and radiation properties.Their popularity is due in part to their versatility, as they can efficiently provide a directional radiation pattern (axial mode) or an omnidirectional pattern (normal mode), specific polarization (linear, circular, or elliptical), and low manufacturing cost, making them suitable for various wireless communication systems (KRAUS, 1988; VOLAKIS, 2007; BALANIS, 2016). They are considered great options for wireless communication systems, satellite communication (LAQUERBE; FRAGNIER, 2022), medical devices (FAERBER et al., 2018),GNSS antennas (STROJNY; ROJAS, 2014), CubeSat telemetry (CHE et al., 2019; ERNEST et al., 2015; ABULGASEM et al., 2021), among others.

Firstly before into the introduces the Additive Manufacturing (AM) and your impact on antenna fabrication, it's essential to understand the inherent complexities involved in constructing these antennas using traditional manufacturing methods. Antennas, especially those with complex geometries and precise specifications, often require frequently processes such as machining to achieve their final form. These conventional manufacturing techniques not only entail significant time and resources but also presented limitations in realizing complex antenna designs. Moreover, the production of antennas with precise dimensions and complex structures demands meticulous attention to detail and expertise in material handling and shaping. These challenges underscore the need for innovative approaches that can streamline the manufacturing process while maintaining the desired quality and performance of antennas. In this context, the emergence of Additive Manufacturing presents a paradigm shift in antenna fabrication, offering a novel solution to overcome the limitations of traditional manufacturing methods. By enabling the direct production of antennas from digital designs, AM provides unprecedented flexibility and efficiency in realizing complex antenna geometries without the constraints imposed by conventional machining processes. This innovative technology not only accelerates the production process but also facilitates the customization of antennas to meet specific performance requirements.Additionally, AM's capability to fabricate antennas from a variety of materials, including dielectric polymers and metal alloys, further enhances its applicability across diverse antenna applications. In summary, while traditional manufacturing methods pose challenges in constructing antennas with intricate designs, Additive Manufacturing emerges as a disruptive solution that revolutionizes antenna fabrication by providing unmatched versatility, efficiency, and customization capabilities.

Concerning the fabrication process, Additive Manufacturing (AM) stands out as a technique where components are conceived utilizing three-dimensional computer-aided design (CAD) software and produced in three dimensions by layering materials (including dielectric polymers or metal alloys) that are sequentially deposited. Given the enhanced feasibility of crafting components with intricate geometries compared to traditional manufacturing processes necessitating machining for their final form, AM has been increasingly adopted across diverse industrial sectors, spanning automotive, aerospace, medical, and consumer goods.(BABU et al., 2015) described the AM process as a disruptive technology because it challenges many paradigms of conventional manufacturing used in the production and consumption of products.Understanding and comprehending the influence of process parameters on the microstructure, formation of manufacturing defects, and mechanical properties of manufactured products are of great importance for the development of the process, aiding in the improvement of part manufacturing.

1.2 Literature Review

Helical antennas are formed by one or more conductive wires wound in a helical shape with a conductive plane at the base, as illustrated in Figs. 1a and b (BALANIS, 2016, Ch. 10). Antenna parameters characteristics vary depending on the geometry and length of the antenna. Consequently the input impedance and return loss is highly dependent on the pitch angle α_n (see Fig. 1a) and the conductor diameter, especially near the feed point (BALANIS, 2016). The three main operating modes are normal (*broaside*), with an omnidirectional radiation pattern, axial (*end-fire*) with a directional radiation pattern, and conical, representing an intermediate case (KRAUS; Williamson, 1948).

Specifically, in axial mode operation, a helical antenna has a nominal impedance of 140 Ω (KRAUS, 1977). An empirical expression, based on a large number of measurements, was derived (KRAUS, 1947) and expressed in the form $Z_R \approx 140\,(C/\lambda_0)$ (BALANIS, 2012), where S is the distance between the helices and λ_0 is the central wavelength of the operating band. The condition close to the optimum for axial mode operation with circular polarization is $S/\lambda_0 = 1$, resulting in $Z_R \approx 140\Omega$ at the central frequency f_0. A simple method to reduce this input impedance and improve impedance matching with standard 50Ω connectors is to increase the wire diameter. Consequently, there is a significant reduction in gain, especially at higher frequencies, reducing the antenna's operating bandwidth (KRAUS, 1977).

When the diameter of the wire is increased, the resistance of the antenna decreases, as resistance is inversely proportional to the cross-sectional area of the conductor. This results in a reduction in the antenna's input impedance, making it more compatible with standard 50 Ω connectors. However, this reduction in input impedance is usually accompanied by a decrease in antenna efficiency, especially at higher frequencies. This is because the increase in wire diameter also increases the capacitance distributed along the antenna, which can lead to unwanted high-frequency resonance. As a result, the operating bandwidth of the antenna can be compromised, resulting in a reduction in gain, especially at higher frequencies (KRAUS, 1977). Therefore, although increasing the wire diameter can improve impedance matching with standard 50 Ω connectors, it can result in a reduction in the antenna's bandwidth and gain, which should be carefully considered when designing and optimizing antennas.

The basic principles of axial mode operation in a helical antenna were established by Kraus in (KRAUS, 1947) and (KRAUS, 1950). In (KRAUS; Williamson, 1948), approximate expressions for the radiation pattern of a single helix and an array of them were derived. In (KRAUS, 1948), it was shown that over a wide frequency range, the radiation pattern, circular polarization, and input impedance are relatively stable, characterizing broadband behavior. The normal operation mode, with circular polarization and maximum radiation orthogonal to the helix axis, was presented in (WHEELER, 1947).

In (KING; WONG, 1980), King and Wong presented the gain characteristics of antennas with 5 to 35 helices and showed that the maximum gain is a function of the number of helices, and the rate of gain increase is a function of the operating frequency. A technique for increasing gain across the band proposed in (WONG; KING, 1979) describes the antenna as a combination of helices with non-uniform helix diameters, achieving a bandwidth twice as large as the conventional form. In (NAKANO; SAMADA; YAMAUCHI, 1986), a parasitic helix was used in an antenna operating in axial mode, obtaining an increase of over 1 dB in gain.

The conventional geometry of helical antennas has a uniform pitch angle (see Fig. 1a). In (CHEN et al., 2007a), the idea is generalized by producing a model with a non-uniform pitch angle generated by exponential spacing between the helices. Numerical and experimental results showed an operating bandwidth 58.6% larger than the conventional geometry. In (K.Jimisha; Kumar, 2012), the idea is explored using an optimization algorithm (PSO - Particle Swarm Optimization) for the optimal choice of the distance between the helices. Numerical analyses show better gain performance versus the number of turns than the conventional model. In (DJORDJEVIC; ZAJIC; ILIC, 2006), using optimization algorithms again, it is shown that the geometry and dimensions of the ground plane have a significant influence on the antenna's performance, and confirms the adequate selection of the size and shape of ground conductor can enhance the gain of the helical antenna. Recently, in (KANG et al., 2020), both ideas, non-uniform pitch angle and non-circular conductive plane, are applied together to construct a conical helical antenna in the 156 MHz range and the percent bandwidth of approximately 8.97%.

An alternative approach to improving the performance of the in-band gain is to work with one more degree of freedom in the generation of the non-uniformity in the *pitch* angle, varying the diameter of the helix and the distance between them (see Fig. 1c). In addition, the diameter of the straight section of the conductor can be varied, using, for example, a wire with a larger diameter at the base of the antenna and a smaller one at

Figure 1. Helical antennas: (a) Standard model (uniform pitch angle); (b) Non-uniform pitch angle model (variable spacing between helices); (c) Non-uniform pitch angle model (variable spacing and diameter of the helices); and (d) Non-uniform pitch angle model (variable spacing, diameter and wire cross-section of the helices)

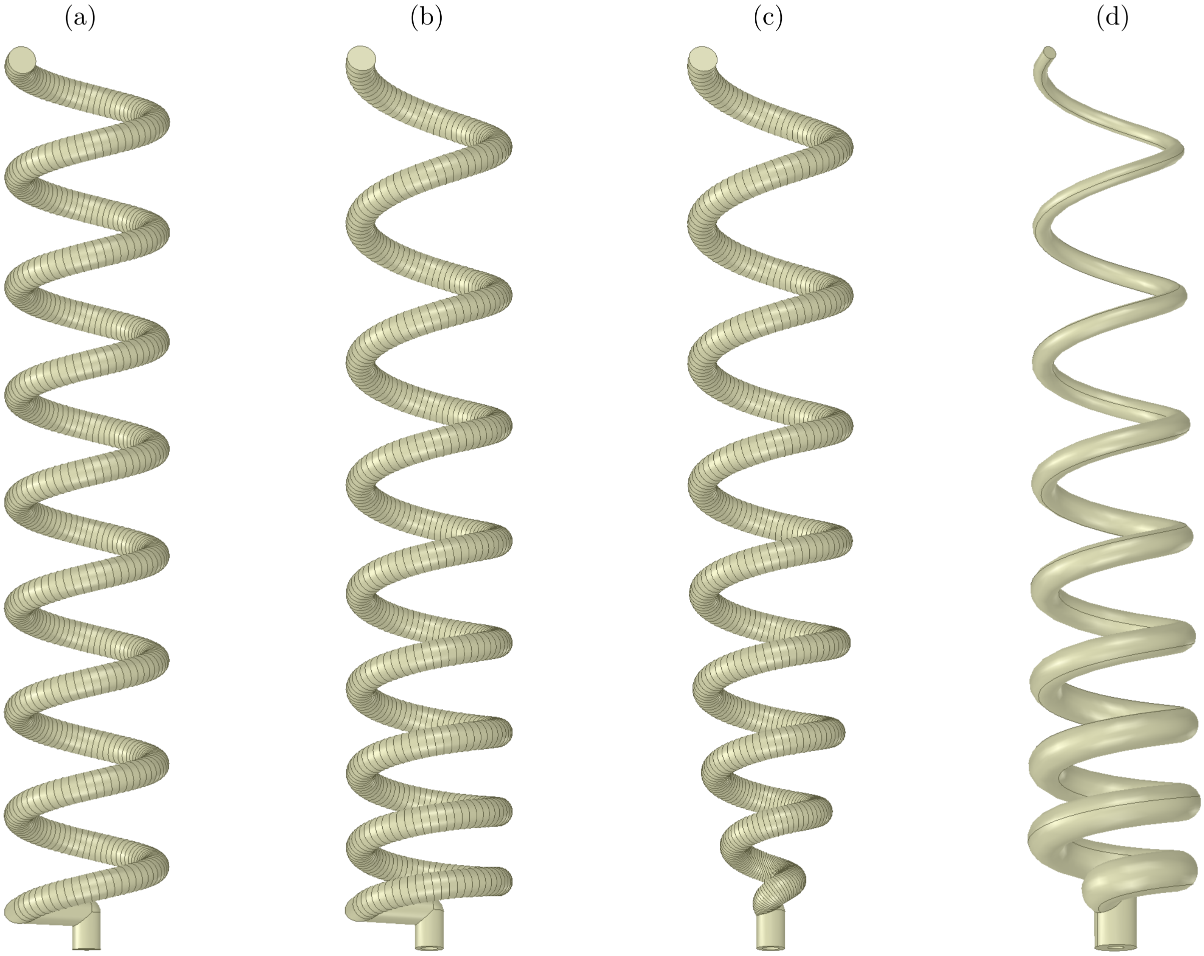

Source: Prepared by the author, 2024

the end (see Fig. 1d).

In the pursuit of enhancing the performance of helical antennas, researchers have continuously explored innovative approaches beyond conventional design methodologies. One such alternative strategy revolves around the manipulation of additional degrees of freedom in the generation of non-uniformity within the antenna structure. This entails varying not only the pitch angle but also the diameter of the helix and the distance between adjacent turns. By incorporating these additional parameters into the design process, a broader design space is opened, offering greater flexibility and potential for performance optimization. This approach aims to tailor the antenna geometry more precisely to the specific requirements of the application, thereby potentially improving key performance metrics such as gain and bandwidth. Furthermore, the utilization of multiple degrees of freedom allows for a more flexible and sophisticated design optimization process, which may lead to superior antenna performance compared to traditional methods. Thus, exploring this alternative approach holds significant promise for advancing the state-of-the-art in helical antenna design and unlocking new possibilities for meeting the evolving demands of wireless communication systems.

The main difficulty with this proposal is the construction. The conventional method of construction by winding does not allow the thickness of the wire to be changed continuously. An alternative to tackle this problem is to use the process of additive manufacturing (AM) of metals with selective laser melting (BABU et al., 2015). Recently, several authors have used the technique to build antennas with complex geometries (BYERS; BARR, 2018), (DORLé et al., 2018), (FOGED et al., 2018) and (GARCíA-MARíN et al., 2018).This innovative approach enables the fabrication of helical antennas with varying wire thickness and intricate geometries that are challenging or impossible to achieve using traditional manufacturing methods. By harnessing the capabilities of additive manufacturing, researchers can explore novel designs and optimize antenna performance, opening up new avenues for advancements in helical antenna technology.

Over the last years, several variations of the canonical cylindrical helical antenna with a ground plane, introduced in (KRAUS, 1949), have been proposed. Configurations such as bifilars (NAKANO; YAMAUCHI, 1986; STROJNY; ROJAS, 2014), quadrifilars (HOSSEINI; HAKKAK; REZAEI, 2005; BYUN; CHOO; KIM, 2015), and multifilars (SHATROV; SIVOV; CHUPRIN, 1994; DOBBINS; ROGERS, 2001) have been introduced. Monofilar helical antenna arrays have been introduced to increase gain by controlling the current distribution along the antenna. However, these approaches introduce complexity in the feeding system compared to the normal monofilar configuration, leading to higher manufacturing costs.

To improve performance, the geometry of a single-wire helix can be changed as an alternative to helix arrays.(DYSON, 1965), (CHATTERJEE, 1953),and (NAKANO; MIKAWA; YAMAUCHI, 1985) investigated the conical helix configuration (rather than cylindrical). In contrast to a typical cylindrical helix, the non-uniform diameter of the coils over the length of the helix permits the maintenance of the axial mode of radiation over a wider bandwidth. The low pitch angle conical helix arrangement has been shown to be effective in controlling the current distribution along the wire, which yields a broadband characteristic of the input impedance. In the study by (CHEN et al., 2007b), a circularly polarized helical antenna with exponential spacing between the coils exhibited a larger axial ratio bandwidth than a helix with conventional linear spacing. More recently, in a work by (DINKIć et al., 2019), a systematic analysis of the effect of non-uniform spacing in helical antennas was conducted. Through numerical optimization, a comprehensive database of helical antennas with optimized non-uniform spacing was compiled, and simple analytical equations for design were presented. (YANG et al., 2008) investigated a similar axial mode helical antenna with a variable tilt angle but with elliptical coil cross-sections to improve radiation.

In the exploration of antenna design, optimization algorithms grounded in artificial intelligence (AI) architectures have garnered significant attention (WU; WANG; HONG, 2020; CUI et al., 2020; LI et al., 2022). This adoption has spurred the development of novel antennas boasting intricate geometries and exceptional electromagnetic properties. For instance, within the domain of helical antennas, ref:peng2011 employed bespoke genetic algorithms to numerically investigate a conical helix antenna featuring a metallic ground plane. Their findings demonstrated that inducing an equivalent inductive conduction to the coil wire can enhance broadband characteristics and lead to a reduced antenna footprint. Nonetheless, the aforementioned shape optimization remains contingent upon the utilization of advanced manufacturing processes. Recent advancements in additive manufacturing have, however, revolutionized the production of antennas with intricate forms, utilizing both dielectric and metallic materials. The transformative potential of additive manufacturing technology in antenna engineering lies in its ability to facilitate the realization of complex structures with precision, thus enabling the customization of antenna designs tailored to specific application requirements derived from optimization algorithms. The attainment of intricate geometries via additive manufacturing unlocks additional degrees of freedom in antenna geometry, thereby affording greater control parameters in the optimization process.

In earlier studies (KIM, 2014; TAWK, 2020; GHASSEMIPARVIN; GHALICHECHIAN, 2020; BENECK et al., 2022), instances of 3D printed helical-like antennas were showcased, with helices fabricated through a combination of a 3D polymer printer and metal coating. However, in this paper, we adopt a distinct approach and investigate the feasibility of metal additive manufacturing (MAM) for producing a monofilar helical antenna. Departing from the conventional two-step process involving polymer resin construction followed by metallization, our methodology leverages MAM directly.

Additional related studies leveraging 3D-printed technology are documented in (CHEN et al., 2021; HU et al., 2022), focusing on Yagi-Uda-like arrays of helical elements. Moreover, in (PANUSCH et al., 2022), the utilization of 3D printing is explored for waveguide-like excitation of helical antennas.

1.3 Objectives and Contributions

In this work we present a generalized helical antenna that incorporates non-uniform helix diameters, non-uniform helix spacing, and non-uniform wire cross-section. By leveraging the additional degrees of freedom in geometry, we optimize the antenna performance in the X-band. The intricate form of the helix antenna, particularly its non-uniform wire cross-section, renders traditional CNC machining with aluminum alloys inadequate. The fabrication process utilizes Maraging steel, known for its durable mechanical structure that can support helices independently, eliminating the necessity for dielectric support structures.

Moreover, the employment of Maraging steel enables the antenna to endure extreme environments characterized by temperature fluctuations without experiencing notable deformation, a stark contrast to polymer alternatives. This aspect is critical, as plastic deformation can adversely affect the antenna's shape and radiation properties. Additionally, Maraging steel demonstrates outstanding corrosion resistance (AVELINO et al., 2018) and mechanical robustness (SANTOS et al., 2022), thereby augmenting the antenna's overall effectiveness and longevity.

The utilization of Metal Additive Manufacturing (MAM) technology in antenna development offers significant advantages, particularly in the design of compact antennas for miniaturized spacecraft (such as pico and nanosatellites) and conventional satellites. Metal Additive Manufacturing (MAM) presents a primary advantage over traditional machining techniques by enabling the production of intricate, lightweight structures without the need for support materials.

One of the notable benefits of Metal Additive Manufacturing (MAM) is its capability to fabricate helical antennas without the necessity for supports typically required in conventional designs employing wire or curved tubes. Moreover, Metal Additive Manufacturing (MAM) empowers the creation of geometries that may be unattainable or impractical with traditional manufacturing methods. For instance, the fabrication of helical geometries with varied cross-sections is feasible, thus opening up novel avenues for antenna design. This enables the integration of complex features aimed at enhancing performance, reducing size, and potentially mitigating production costs.(PENCHEL et al., 2024)

The primary contribution of this study is in advancing the mathematical representation for helical antennas, particularly focusing on the incorporation of a tapered cross-section wire. This research propels the evolution of monofilar helical antennas by introducing non-uniform helix diameters, spacings, and wire cross-sections, thereby presenting novel avenues for optimization beyond conventional design methodologies. In our view, the complete fusion of these various characteristics, namely the variation of the wire cross-section, presents a unique facet of this study that has received little attention in previous research. The use of metal additive manufacturing (MAM) technology allows for the creation of a tapered wire cross-section that is used to influence the antenna's current distribution, thereby improving impedance matching and radiation attributes.

Part of the results presented in this dissertation were published in the following journal article:

Rafael A. Penchel, Nicholas F. Martins, Ivan Aldaya, José A. de Oliveira, Mirian P. dos Santos, Andre L. Jardini, Julian Avila, Guilherme S. Rosa, "Performance evaluation of a novel monofilar helical antenna with tapered cross-section wire fabricated via metal additive manufacturing", *AEU - International Journal of Electronics and Communications*, 2023, 155085, ISSN 1434-8411, https://doi.org/10.1016/j.aeue.2023.155085.

1.4 Organization of work

The rest of this dissertation is organized as follows: Charpter 2 presents the novel formulation of a generalized nonofilar helix antenna, Chapter. 3, in Sec. 3.1 describes the fabrication details of the MAM employed in this work and numerical and experimental results are presented in Sec. 3.2. Sec. 3.3 investigates the underlying factors contributing to the superior performance of the tapered-wire antenna compared to other configurations utilizing uniform-cross-section wires. Finally, concluding remarks are presented in Sec. 4.

2 Helical antenna design

2.1 Generalized helix design

The proposed configuration of the helical antenna is described in Fig. 2.The structure under examination exhibits three primary components: the metallic helical wire (with a non-uniform radius), a reflective ground-plane, and the coaxial waveguide feeder. In this particular model, the helix assembly is composed by sequentially linking a series of N metallic coils.

In general, a standard helix antenna can be expressed by parametric equations as follows:

$$x(\ell) = R\cos(2\pi\, N\,\ell) \tag{2.1}$$

$$y(\ell) = R\sin(2\pi\, N\,\ell) \tag{2.2}$$

$$z(\ell) = H\ell \tag{2.3}$$

where ℓ denotes the normalized length of the wire, which ranges from 0 to 1. The parameter $R = D/2$ represents the maximum radius of the helix coils, N denotes the number of turns (coils), and H indicates the total height of the helix along the antenna axis.

In the generalized model proposed in this work, the helix is constructed by a series of N sequentially concatenated metallic coils. The length of each coil is denoted as $L_1, L_2, ..., L_N$, and the spacing between the coils is represented by $S_1, S_2, ..., S_N$. Moreover, the diameter of each coil varies along the antenna axis (z-axis in Fig. 2) and is given by $D_1, D_2, ..., D_N$. The mathematical representation proposed on this work for generalized helix is described in Cylindrical coordinates (ρ, ϕ, z) by

$$\rho(\ell) = R\left(\frac{e^{\alpha_\rho\, z(\ell)/L} - 1}{e^{\alpha_\rho} - 1}\right), \tag{2.4}$$

$$\phi(\ell) = 2\pi\, N\,\ell, \tag{2.5}$$

$$z(\ell) = H\left(\frac{e^{\alpha_z\,\ell} - 1}{e^{\alpha_z} - 1}\right). \tag{2.6}$$

In Cartesian coordinates (x, y, z), the helix is described by means of

$$x(\ell) = R\left(\frac{e^{\alpha_\rho\, z(\ell)/L} - 1}{e^{\alpha_\rho} - 1}\right)\cos(2\pi\, N\,\ell), \tag{2.7}$$

$$y(\ell) = R\left(\frac{e^{\alpha_\rho\, z(\ell)/L} - 1}{e^{\alpha_\rho} - 1}\right)\sin(2\pi\, N\,\ell), \tag{2.8}$$

$$z(\ell) = H\left(\frac{e^{\alpha_z\,\ell} - 1}{e^{\alpha_z} - 1}\right). \tag{2.9}$$

The parameters α_ρ and α_z are employed to manage the radial and axial characteristics of the helix. Moreover, in contrast to typical models documented in existing literature, the dimensions of the wire's cross-section $(d_1, d_2, ..., d_N)$ vary throughout the helix's length.

Figure 2. Geometry of generalized helical antenna with tapered cross-section wire.

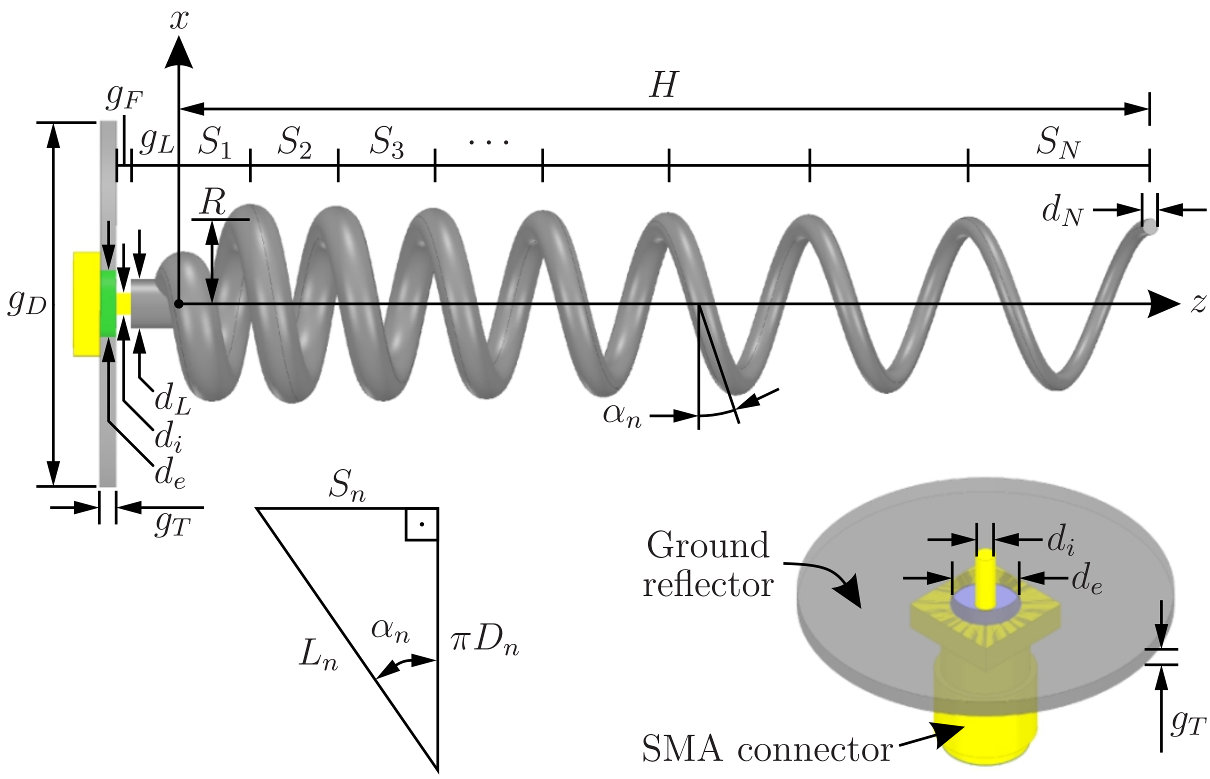

Source: Prepared by the author, 2024

To demonstrate the assortment of helix configurations attainable with varying values of α_ρ and α_z, Fig. 3(a)-(i) showcases various helix geometries using $R = 4$ cm, $L = 6$ cm, and $N = 8$. In the helix scenarios introduced in Fig. 3(b), (e), and (h), we set $\alpha_z = 0$ to maintain a constant distance S_n between the coils. When $\alpha_z < 0$ (Fig. 3(a), (d), and (g)), the distance S_n decreases near the top of the helix, while for $\alpha_z > 0$ (Fig. 3(c), (f), and (i)), S_n increases at the top. Conversely, if we set $\alpha_\rho = 0$ (Fig. 3(d), (e), and (f)), the helix exhibits a linear radial profile. A negative value of α_ρ results in a concave radial profile (Fig. 3(a), (b), and (c)), while a positive value yields a convex radial profile (Fig. 3(g), (h), and (i)).

There exist some notable special cases. In the scenario where $\alpha_\rho \to -\infty$ and $\alpha_z = 0$, equations (2.4)–(2.6) simplify to the expressions for a uniformly spaced standard cylindrical helix (similar to the illustration in Fig. 3(b)), which are commonly referenced in existing literature (KRAUS, 1949; NAKANO; YAMAUCHI, 1986; BALANIS, 2008). It is worth mentioning that, as $\alpha_\rho \to -\infty$, we have:

$$\lim_{\alpha_\rho \to -\infty} \left(\frac{e^{\alpha_\rho z(\ell)/L} - 1}{e^{\alpha_\rho} - 1} \right) = \left(\frac{0-1}{0-1} \right) = 1, \tag{2.10}$$

and the equation (2.7) and (2.8) take the form of (2.1) and (2.2), respectively. Similarly, we compute the limit

$$\lim_{\alpha_z \to 0} \left(\frac{e^{\alpha_z \ell} - 1}{e^{\alpha_z} - 1} \right) \tag{2.11}$$

as α_z approaches zero using the L'Hôpital's rule. Firstly, we observe that as α_z approaches zero, both $e^{\alpha_z \ell}$ and e^{α_z} approach 1. Therefore, we can rewrite the expression as:

$$\lim_{\alpha_z \to 0} \left[\frac{\frac{d}{d\alpha_z}(e^{\alpha_z \ell} - 1)}{\frac{d}{d\alpha_z}(e^{\alpha_z} - 1)} \right] \tag{2.12}$$

Applying L'Hôpital's rule:

$$\lim_{\alpha_z \to 0} \left(\frac{e^{\alpha_z \ell} - 1}{e^{\alpha_z} - 1} \right) = \lim_{\alpha_z \to 0} \left(\frac{\ell e^{\alpha_z \ell}}{e^{\alpha_z}} \right) \tag{2.13}$$

As α_z approaches zero, $e^{\alpha_z \ell}$ approaches 1 and e^{α_z} approaches 1, therefore the limit becomes:

$$\lim_{\alpha_z \to 0} \left(\frac{e^{\alpha_z \ell} - 1}{e^{\alpha_z} - 1} \right) = \frac{\ell}{1} = \ell \tag{2.14}$$

Hence, the equation (2.9) takes the form of (2.3).

For $\alpha_\rho = 0$ and $\alpha_z = 0$, we obtain the geometry of a conical helical antenna as described in references (DOBBINS; ROGERS, 2001; CHATTERJEE, 1953; NAKANO; MIKAWA; YAMAUCHI, 1985; ZHOU et al., 2016; ERNEST et al., 2015). The pitch angle becomes uniform when $\alpha_z = 0$, and the coil radius becomes uniform when $\alpha_\rho = -\infty$.

Figure 3. Generalized helices examples considering $R = 2$ cm, $H = 6$ cm, $N = 8$ turns, and with (a) $\alpha_\rho = -10^3, \alpha_z = -2.5$; (b) $\alpha_\rho = -10^2, \alpha_z = 0.0$; (c) $\alpha_\rho = -10, \alpha_z = 2.5$; (d) $\alpha_\rho = 0.0, \alpha_z = -2.5$; (e) $\alpha_\rho = 0.0, \alpha_z = 0.0$; (f) $\alpha_\rho = 0.0, \alpha_z = 2.5$; (g) $\alpha_\rho = 2.5, \alpha_z = -2.5$; (h) $\alpha_\rho = 5.0, \alpha_z = 0.0$; (i) $\alpha_\rho = 10, \alpha_z = 2.5$. The small circle represents the feeding point where the 3.5 mm SMA coaxial connector is attached. The dashed-line represents the helix radial profile over $\phi = 0$.

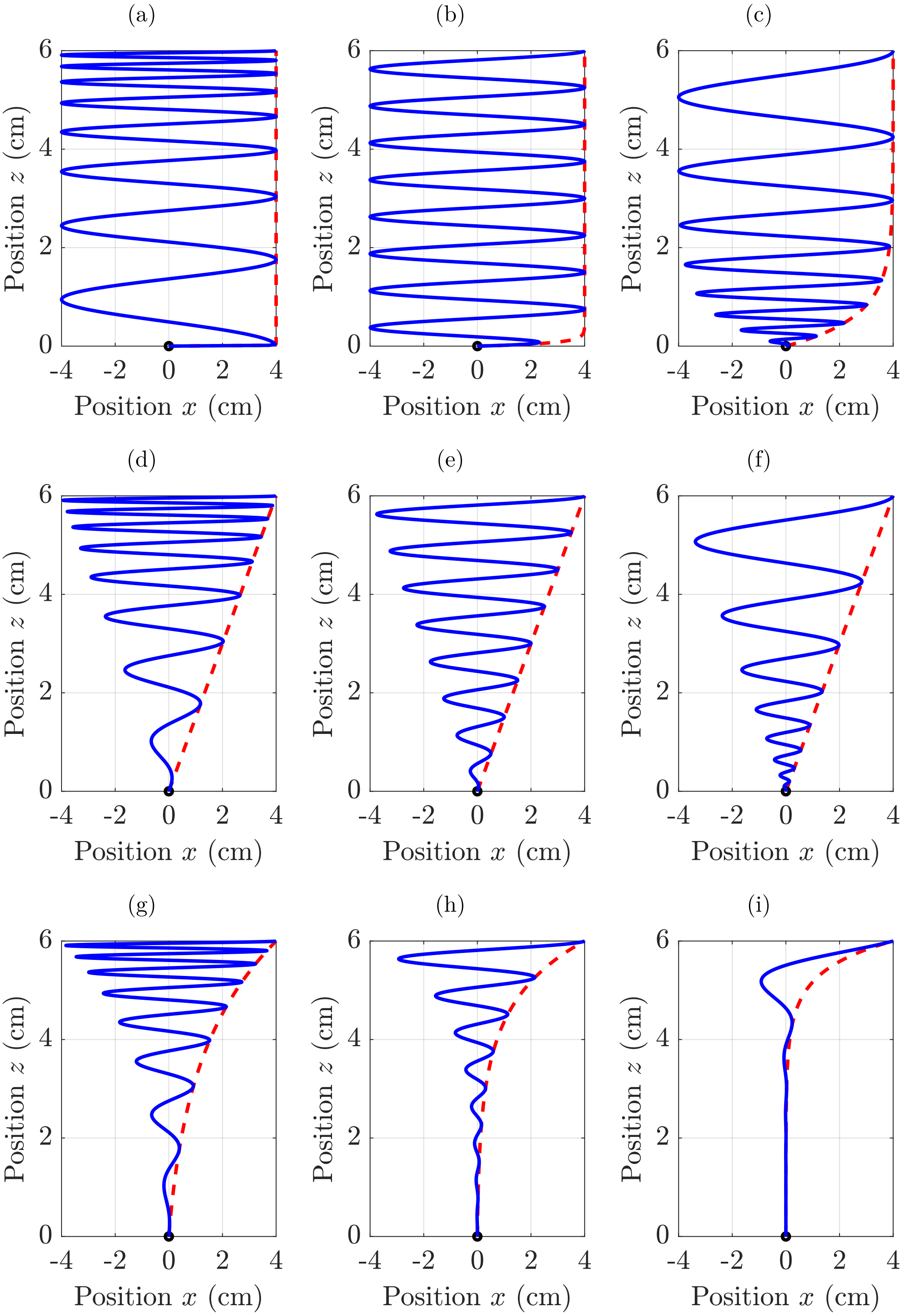

Source: Prepared by the author, 2024

2.2 Parametric Analysis

In this section, we present the parametric analysis carried out on the g_L,g_D and d_N parameters to investigate the performance of the proposed helical antenna.This initial stage allowed us to lay a solid foundation for the more in-depth analysis that was to follow. ANSYS Electronics Desktop software (ANSYS, Inc., 2023) was used to conduct these analyses, providing an in-depth understanding of the variations in these parameters and their impact on the antenna's characteristics.

Table 1. Parameters of the prototype model antenna

Parameter	Prototype Model
N	8
H(mm)	60
R(mm)	4.775
α_ρ	-10^4
α_z	0.0
g_L(mm)	3.0
g_F(mm)	0.5
g_T(mm)	2.0
g_D(mm)	25
d_i(mm)	1.27
d_e(mm)	4.2
d_L(mm)	1.2
d_N(mm)	1.2

Source: Prepared by the author, 2024

ANSYS software was chosen because of its advanced capacity for simulating and analyzing complex structures. Initially, simulations were carried out using the design parameters. Subsequently, parameterizations were carried out to explore the different operating conditions. The parameters used for the initial antenna prototype are provided in Table 1. Initially, simulations were conducted using these predefined parameters to establish a baseline performance. Subsequently, parameterizations were carried out to explore various operating conditions, allowing for a comprehensive analysis of the antenna's behavior under different scenarios. The detailed results of the parametric analysis for g_L, g_D, and d_N will be discussed in the following pages.The detailed results of the parametric analysis for g_L,g_D and d_N will be presented in this section. Each parameter will be discussed separately, highlighting the significant findings and trends observed during the simulations.

In the figure 4 shows the results of the simulation focused on parameter S_{11}. Three cases are shown with different parameterizations for the diameter of the wire's cross-section d_N, the distance between the ground plane and the first helix g_L and the diameter of reflecting ground plane g_D. Each graph highlights the variation in S_{11} in response to these parameterizations,

Figure 4. Results of the simulation focused on parameter S_{11}. Three cases are shown with different parameterizations: (a) Original Antenna Design; (b) Diameter of the reflecting ground plane g_D; (c) Distance between the ground plane and the first helix g_L; (d) Diameter of the helixes d_N;

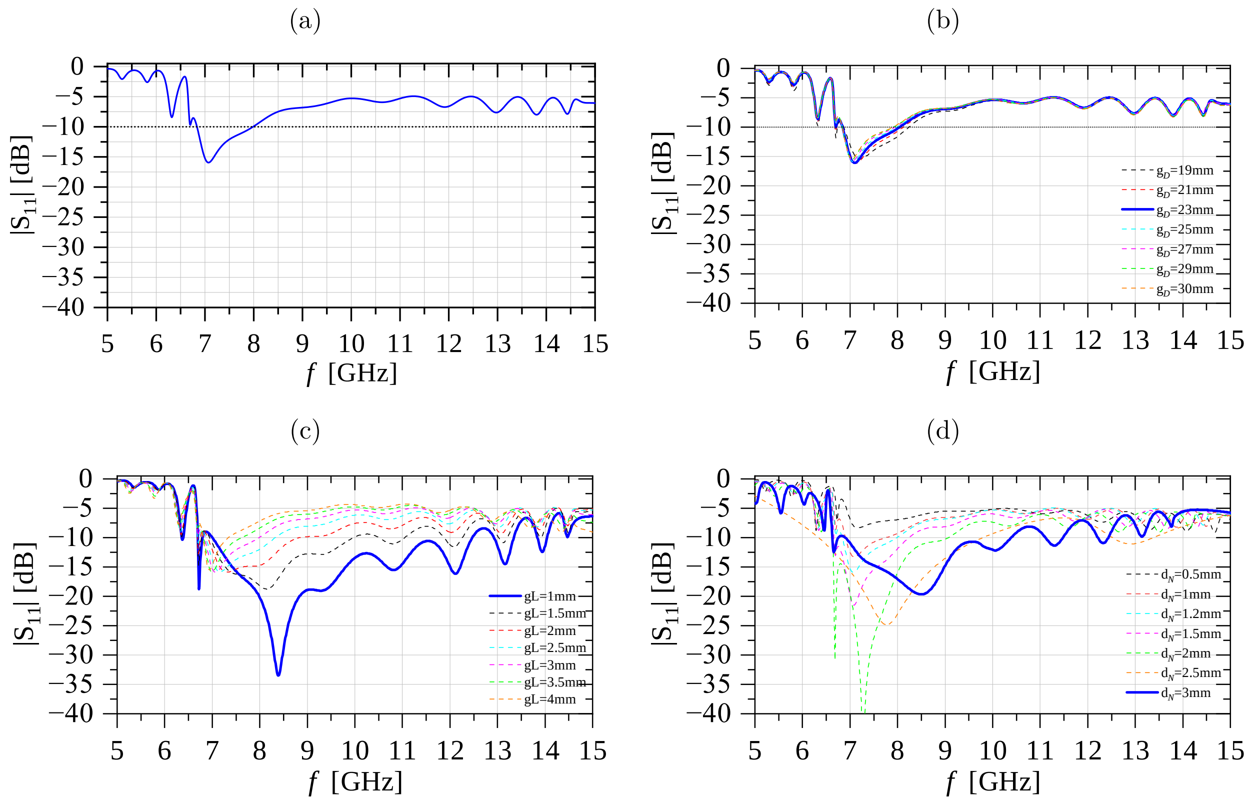

Source: Prepared by the author, 2024

By performing the parameterizations of g_L and d_N in the simulations, we observed that it is possible to maximize the reflection coefficient S_{11} by slightly increasing the diameter of the coil or reducing the length g_L. These modifications provide significant optimization and and a significant increase in channel bandwidth compared to the initial design parameters. In contrast to the previous case, even when varying the parameter g_D, in the simulations, we observed that the reflection coefficient remained very close to that of the antenna's original design, as shown in figure 4.

When analyzing the Z_{11} results, as shown in figure 5 , we observed that, once again, the g_D parameter behaved consistently, remaining very close to the values of the antenna's original design, even after the parameterizations were made.This may be because the antenna's initial design value may already be close to the optimum configuration for the specific project conditions. Thus, even with variations, the antenna's performance can remain efficient.

Analyzing the parametrization for d_N and g_L in relation to the Z_{11} and S_{11} results, we notice a similar behavior. The results of the d_N and g_L parametrics converge and optimize to values close to 3 mm and 1 mm respectively for both Z_{11} and S_{11}. It is crucial

Figure 5. Results of the simulation focused on parameter Z_{11}. Three cases are shown with different parameterizations: (a) Original Antenna Design; (b) Diameter of the reflecting ground plane g_D; (c) Distance between the ground plane and the first helix g_L; (d) Diameter of the helixes d_N;

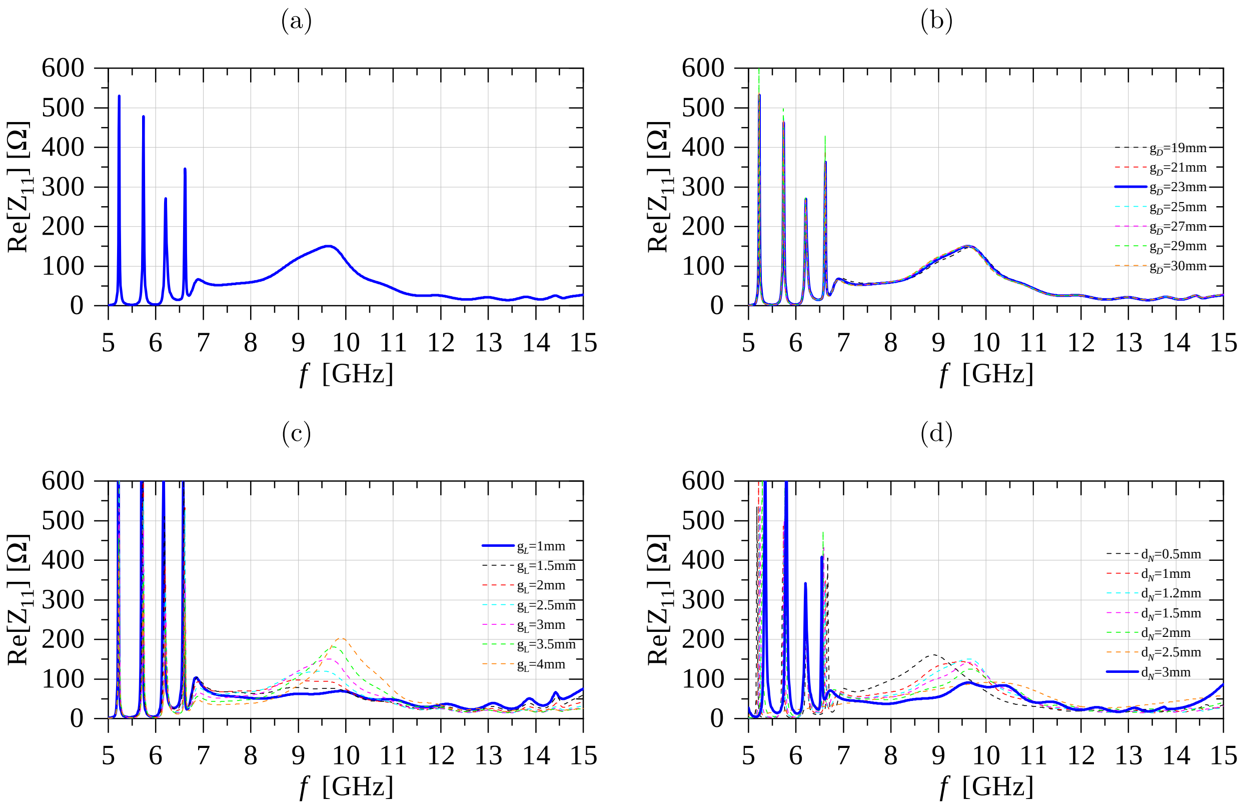

Source: Prepared by the author, 2024

to note that these two parameters directly influence the channel's bandwidth. We observed a significant improvement in channel bandwidth by varying d_N and g_L. These optimizations resulted in a significant improvement in the channel's bandwidth, providing improved data transmission capacity compared to the initial design.

When analyzing peak gain, as shown in figure 6, the parameters g_D, d_N and g_L performed differently. Increasing the diameter of the ground plane g_D is shown to have a positive influence on peak gain, indicating a direct correlation between the size of the ground plane and the increase in gain.For g_L, we observed a little increase in gain, as well as for d_N, both resulting in gains slightly higher than the original design of the antenna. These increases are relatively small due to the characteristics of the parameters in question, which do not exert a significant influence on the antenna's peak gain. The increase in gain stems from the intrinsic characteristics of the g_L and d_N parameters, which are more related to impedance matching and antenna efficiency than to peak gain. Therefore, while these parameterizations impact bandwidth and efficiency, they do not have a substantial effect on the peak gain of the antenna.

During the analysis of the helical antenna's parameters, we observed different patterns in relation to the reflection coefficient S_{11}, the impedance Z_{11}, and the Peak Gain. The variations in g_D, g_L, and d_N exhibited distinct impacts on these antenna performance metrics. While g_D showed minimal influence on S_{11}, and Z_{11}, g_L and d_N had noticeable effects, particularly on bandwidth and efficiency. g_L demonstrated a slight increase in gain, while d_N resulted in similar gains to the antenna's original design. However, these gains were relatively small, attributed to the inherent characteristics of these parameters, which are more closely related to impedance matching and antenna efficiency than peak gain.

The utilization of uniform thin wires has been observed to confer favorable radiation characteristics, particularly with respect to achieving advantageous gain in co-polarization and effective rejection in cross-polarization. However, it is noteworthy that the impedance matching of these antennas becomes compromised under such configurations. This serves as a motivation for conducting a more refined study of alternative antenna models based on the optimized parameters. One such approach involves the use of non-uniform wires, where a larger initial diameter wire's section d_L and a smaller final diameter wire's section d_N are employed to benefit from favorable radiation characteristics while also addressing impedance matching issues. Additionally, this configuration has been observed to increase the bandwidth of the antenna, making it a promising avenue for enhancing overall performance and versatility in various communication scenarios.

2.3 Design and Analysis

To investigate the proposed formulation, due to X-band (8 GHz–12 GHz) being used for radar, satellite communication, and wireless computer networks.We selected three models for evaluation in the X-band , with a central frequency of $f_0 = 10$ GHz (corresponding to a free-space wavelength of approximately $\lambda_0 \approx 30$ mm). These models operate in axial mode and consist of helical antennas with $N = 8$ coils. The three models are as follows:

- Model I) Standard helical antenna with uniform diameter and spacing between coils.
- Model II) Helical antenna with non-uniform diameter and spacing between coils.
- Model III) Helical antenna with non-uniform diameter, cross-section, and spacing between coils.

To achieve circular polarization in the major lobe and excite the axial mode, we adopted a spacing between helices of $S = \lambda_0/4 = 7.5$ mm and a circumference $C = \lambda_0 = 30$ mm for Model I. This reference configuration results in a helix height of $H = 60$ mm and a helix radius of $R = 4.775$ mm. These parameters were selected based

Figure 6. Results of the simulation focused on parameter Peak Gain. Three cases are shown with different parameterizations: (a) Original Antenna Design; (b) Diameter of the reflecting ground plane g_D; (c) Distance between the ground plane and the first helix g_L; (d) Diameter of the helixes d_N;

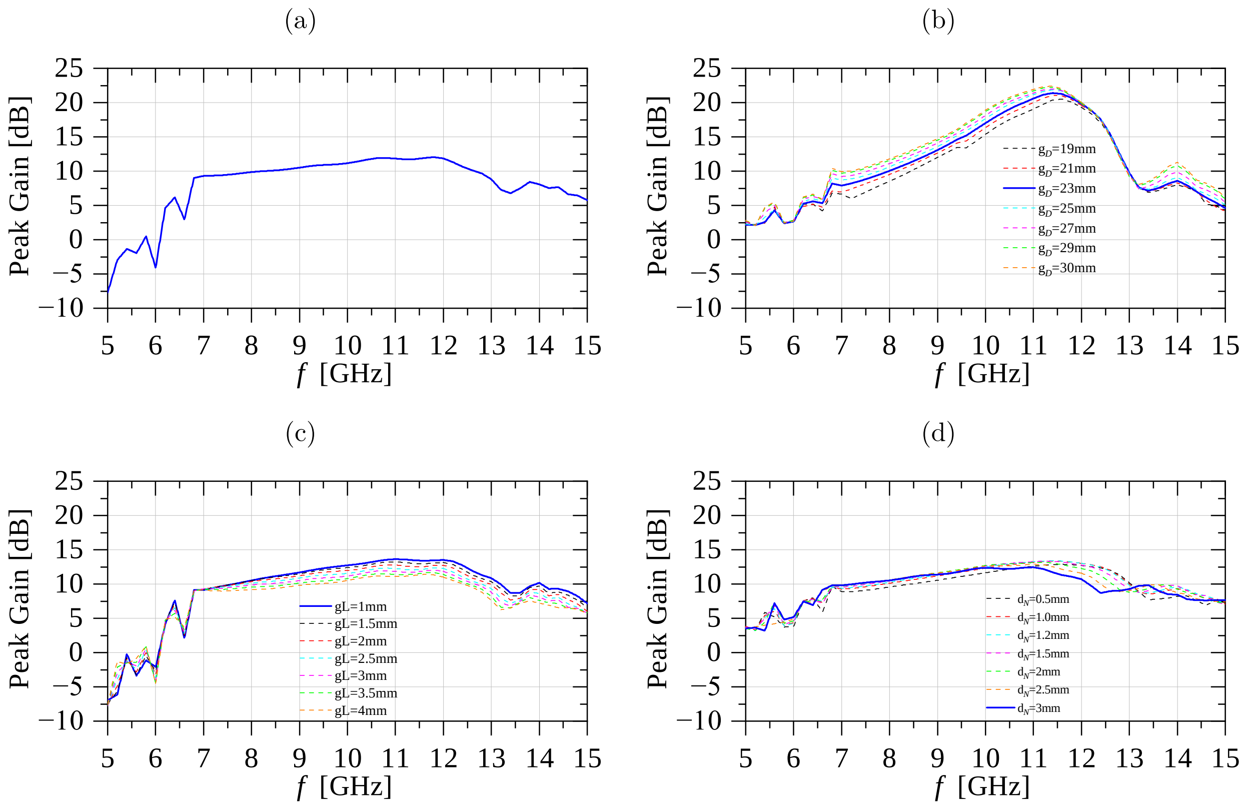

Source: Prepared by the author, 2024

on well-known design formulas for conventional helical antenna design (KRAUS, 1949; BALANIS, 2008).

Strictly speaking, the helix of a standard antenna in mathematical modeling would be obtained by setting $\alpha_\rho = -\infty$, $\alpha_z = 0$. However, these values lead to numerical (removable) singularities in (2.4) and (2.6), which can be avoided by adopting $\alpha_\rho = -10^4$, $\alpha_z = 0.0$ with no significant differences. Thus, the length of each coil (L_n), the distance between the coils (S_n), the coil diameter (D_n), and the pitch angle (α_n) are approximately uniform.

The initial diameter of the helix was chosen to be the same as the diameter of the helix initial section (d_L) (as illustrated in Fig. 2). The diameters of the central pin (d_i) and the hole in the reflector plane (d_e) were chosen to match the dimensions of a commercial SMA connector, specifically the central pin diameter and the dielectric diameter, respectively.

The electromagnetic analyses of the antennas were performed on ANSYS Electronics Desktop, using the finite element method (FEM) solver (ANSYS, Inc., 2023). Optimization algorithms were used to select the best antenna parameters in view of improving the antenna reflection coefficient and the realized gain. Table 2 summarizes the parameters of the designed antennas, whose geometries are compared in Fig. 7.

Table 2. Parameters of the three helical antennas models

Parameter	Model I	Model II	Model III
N	8	8	8
H (mm)	60	60	60
R (mm)	4.775	4.775	4.775
α_ρ	-10^4	-80	-80
α_z	0.0	1.0	1.0
g_L (mm)	3.0	3.0	4.0
g_F (mm)	0.5	0.5	0.5
g_T (mm)	2.0	2.0	2.0
g_D (mm)	25	25	25
d_i (mm)	1.27	1.27	1.27
d_e (mm)	4.2	4.2	4.2
d_L (mm)	2.0	2.0	3.0
d_N (mm)	2.0	2.0	1.0

Source: Prepared by the author, 2024

To ensure a fair comparison between all the models, we kept the parameters N, H, and R (as shown in Table 2) constant for Models II and III. However, we allowed the helix parameters L_n, S_n, D_n, and α_n to vary along the z-axis, by adjusting $\alpha_\rho = -80$ and $\alpha_z = 1$. Although non-uniformly spaced antennas have been documented in the literature, the

Figure 7. Geometry of the helical antennas. (a) Model I. (b) Model II. (c) Model III.

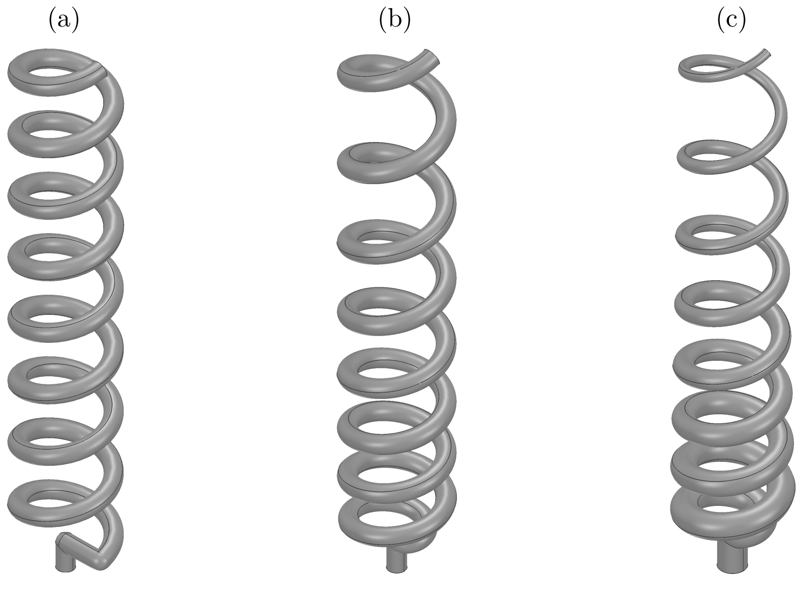

Source: Prepared by the author, 2024

specific form proposed in this work enables a refined treatment of the first helix diameter through the coefficient α_ρ, in the reflection coefficient optimization.

The initial design parameters for the helical antenna models presented here were carefully selected to enhance their impedance matching and radiation characteristics. We employed a combination of empirical methods and simulation-based optimization techniques. For Model I, conventional design formulas for helical antennas were used as a baseline. In Models II and III, we refined parameters such as coil diameters and spacings through an iterative optimization process, guided by the physical limits of the MAM machine and associated mechanical constraints. Specifically, the use of particular values for α_ρ and α_z in Model II led to improved impedance characteristics. Additionally, the optimization results suggested that the use of a non-uniform wire cross-section significantly enhances impedance characteristics and certain aspects of the antenna's radiation performance. These findings are further detailed in Sec. 3.2 and Sec. 3.3.

Model III employs the same helix as Model II but with the innovative feature of a linearly decreasing wire cross-section along the helix axis ℓ. At the start of the helix, located at $\ell = 0$, the wire's cross-sectional radius is $r_L = 1.5$ mm, and at the end of the helix, at $\ell = 1$, the radius is reduced to $r_N = 0.5$ mm. This design strategy has been shown to result in a broadening of the antenna's operating bandwidth. Mathematically, the cross-sectional radius of the wire, denoted as $\rho'(\ell)$, can be expressed as a function of ℓ along the helix by

$$\rho'(\ell) = r_L + \ell(r_N - r_L), \tag{2.15}$$

where $r_L = d_L/2$ and $r_N = d_N/2$.

3 Numerical and Experimental Results

3.1 Fabrication process

A high-resolution additive manufacturing method called Laser Powder Bed Fusion (L-PBF) was used to manufacture all helical antennas. The apparatus used was the EOS 280, which has a 180–200 W laser capacity and a 50 μm powder layer thickness. Nitrogen gas was pumped into the manufacturing chamber to keep oxygen from contaminating it. Using gas-atomized powder, Maraging 18Ni grade 300 steel was produced, with the measured chemical composition of 17.88Ni, 0.001C, 9.0Co, 4.8Mo, 1.1Ti, and 0.1Al (wt%). Following aging heat treatment, this material is renowned for having extremely high mechanical strength. See (PENCHEL et al., 2024; SANTOS et al., 2022) for further information.

The antennas were printed with the building direction perpendicular to the main axis in order to optimize the use of powder material. As a result, the overhanging portions of the helical geometries required support systems. The samples were then removed off the building platform by means of electrical discharge machining. The pieces were finished using 1000/2000 metal sandpaper after the support structures were manually removed during the last manufacturing phase. The constructed models are shown in Fig. 8 both before and after the finishing stage. The final printing stage photos show us that the models have support structures placed beneath the helix with purpose, as well as the characteristic roughness from the MAM process. The main challenge encountered in utilizing L-PBF was identifying an optimal arrangement of support structures for the overhanging parts of the antenna. These support structures are essential to prevent liquid droplets from falling during the fusion of the powder bed of overhanging components. Additionally, once the fusion process is complete, they facilitate thermal transfer towards the lower layers and the building platform. However, the presence of these supporting frameworks may introduce residual stress, potentially leading to the fracture of the manufactured antenna. This was the scenario encountered during our initial two attempts. However, on the third attempt, we achieved successful fabrication of the intended antenna structures by determining the appropriate distribution of support structures.

Microstructural features of the additive manufacturing materials are depicted in Fig. 9. These materials showcase irregular contours and micro melt pools with an approximate size of 0.1 mm. Fig. 9(c) illustrates the presence of martensite laths and growth through multiple melt pools. In the as-built condition, the material exhibits a hardness of 375 Vickers, an ultimate mechanical strength of 1200, and an elongation of approximately 18%, as reported in a previous study by Santos et al. (SANTOS et al., 2022). Microstructural characterization revealed minimal processing defects, with the density

Figure 8. Fabricated helical antennas using the metal additive manufacturing process, showing the antennas before and after the finishing phase. (a) Antenna Model I. (b) Antenna Model II. (c) Antenna Model III. The darker areas behind the helices (before the completion process) represent the support structures necessary for the MAM process.

Source: Prepared by the author, 2024

closely resembling that of conventional wrought steel. It is important to note that these characteristics do not significantly impact the electromagnetic performance of the antennas at X-band, as will be confirmed in the subsequent section.

The intricate shape of the helix antenna, particularly the non-uniform cross-section wire, renders it inappropriate for conventional CNC machining utilizing aluminum-based alloys. Although triangular or square cross-section wires can be generated through CNC threading operations, these geometries substantially deviate from the tapered cylindrical wires envisaged in Antenna Models II and III. Moreover, even manufacturing uniform wires using CNC may lead to deformation owing to the requisite small diameters.

Another evident aspect to consider is that CNC machining commonly utilizes aluminum alloys. Achieving very thin machining with CNC can often prove impractical, but it can be readily achieved through additive manufacturing using steel materials. This approach not only simplifies the manufacturing process but also enables the fabrication of helical antennas without the need for external supports or spacers, thereby enhancing the overall robustness of the antenna.

Figure 9. A MAM-printed wire showing (a) the macrostructure of a thin section accompanied by (b) low magnification and (c) high magnification photos.

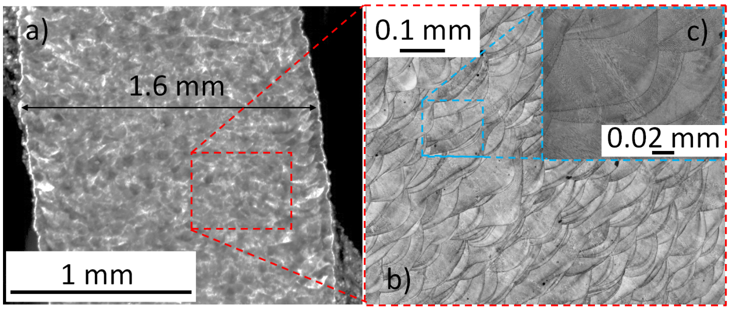

Source: Prepared by the author, 2024

3.2 Simulated and Experimental Results

This section presents the outcomes of the optimized antenna designs, which were developed employing the Finite Element Method (FEM) solver integrated into Ansys HFSS (ANSYS, Inc., 2023), focusing on the three antenna models currently under scrutiny. Electromagnetic characterization took place within an anechoic chamber facilitated by Albatross Projects GmbH, with a Keysight FieldFox Vector Network Analyzer model N995A employed for measurements.

The realized gain of the helical antennas was assessed through the implementation of the two-antenna method, in accordance with the protocol delineated by Balanis (BALANIS, 2016, Sec. 17.4.1). To ensure precision and provide reference data, a set of standard pyramidal horns, along with two Right-Handed Circular Polarization (RHCP) antennas and one Left-Handed Circular Polarization (LHCP) helical antenna, were utilized for calibration and comparative measurements.

Fig. 11 presents the reflection coefficient $|S_{11}|$ of the fabricated helical antennas. A notable agreement was observed between the measurements and the results obtained from the FEM simulations. The passbands were identified using the widely-adopted criterion of $|S_{11}| \leq -10$ dB. Model I, as depicted in Fig. 11(a), showcases a passband from 6.56 GHz to 9.06 GHz, corresponding to a percent bandwidth of approximately 32.01%. Model II, highlighted in Fig. 11(b), exhibits a passband ranging from 6.21 GHz to 11.48 GHz, with a bandwidth of approximately 59.58%. Additionally, Fig. 11(c) presents the results of antenna Model III, revealing a passband spanning from 6.12 GHz to 15 GHz (our upper limit measurement), alongside a bandwidth of approximately 84.09%. This discovery reaffirms that tapering the wire cross-section can effectively enhance the bandwidth characteristic of the helical antenna. Further insights into this matter will be presented in Sec. 3.3.

Minor discrepancies between simulated and measured results, as depicted in Fig. 11, are noted, particularly in frequencies below 7 GHz and above 13 GHz across all compared

Figure 10. Electromagnetic characterization of a manufactured helical antenna. (a) Antenna installed in an anechoic chamber. (b) Detailed view of the helical antenna Model III.

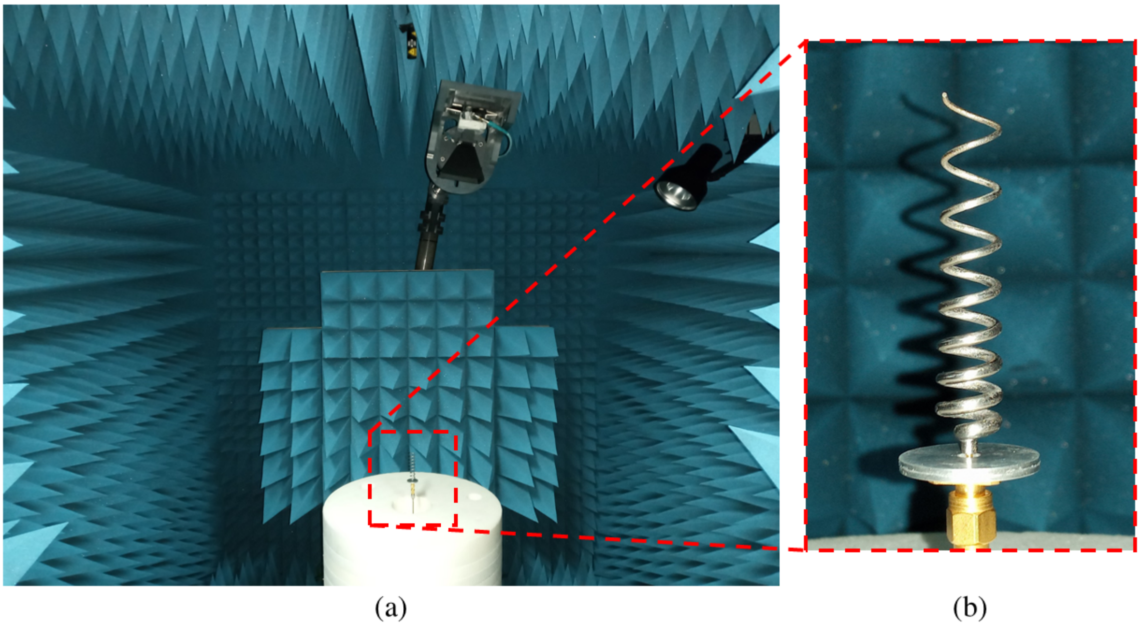

Source: Prepared by the author, 2024

antenna models. Additionally, antenna Model II exhibits a deviation of approximately 3 dB at 8 GHz. These differences are attributed to the typical roughness generated by the MAM process and assembly errors associated with the small 3.5 mm connector at the base of the helices.

The radiation patterns (RHCP and LHCP) in the principal planes ($\phi = 0°$ and $\phi = 90°$) at the limiting and central frequencies of the X band are illustrated in Fig. 12 to Fig. 14. Notably, a robust concordance is observed between the experimental and simulated results within the primary radiation lobe.

Certain disparities between the simulated and measured results are evident in the cross-polar radiation patterns. These discrepancies arise from limitations within our measurement setup, particularly when capturing the low-level signal of the LHCP.

The observed reduction in back lobe as the frequency increases can be attributed to the expanding electrical size of the ground plane.

Fig. 16 displays the measured results of the maximum realized gain for right-handed circular polarization (RHCP). Notably, both Model I and Model II exhibit a gain approximately 1 dB higher than Model III across most of the operating bandwidth. The peak gain of the tapered-wire antennas was 10.8 dBic and varied by less than 2.4 dB along the X band, displaying greater consistency compared to other models.

Figure 11. The reflection coefficient of the manufactured helical antennas is plotted as a function of frequency. The measurement results are represented by solid lines, while the simulation results are represented by dashed lines. The reference level, indicated by dotted lines, corresponds to $|S_{11}| = -10$ dB.

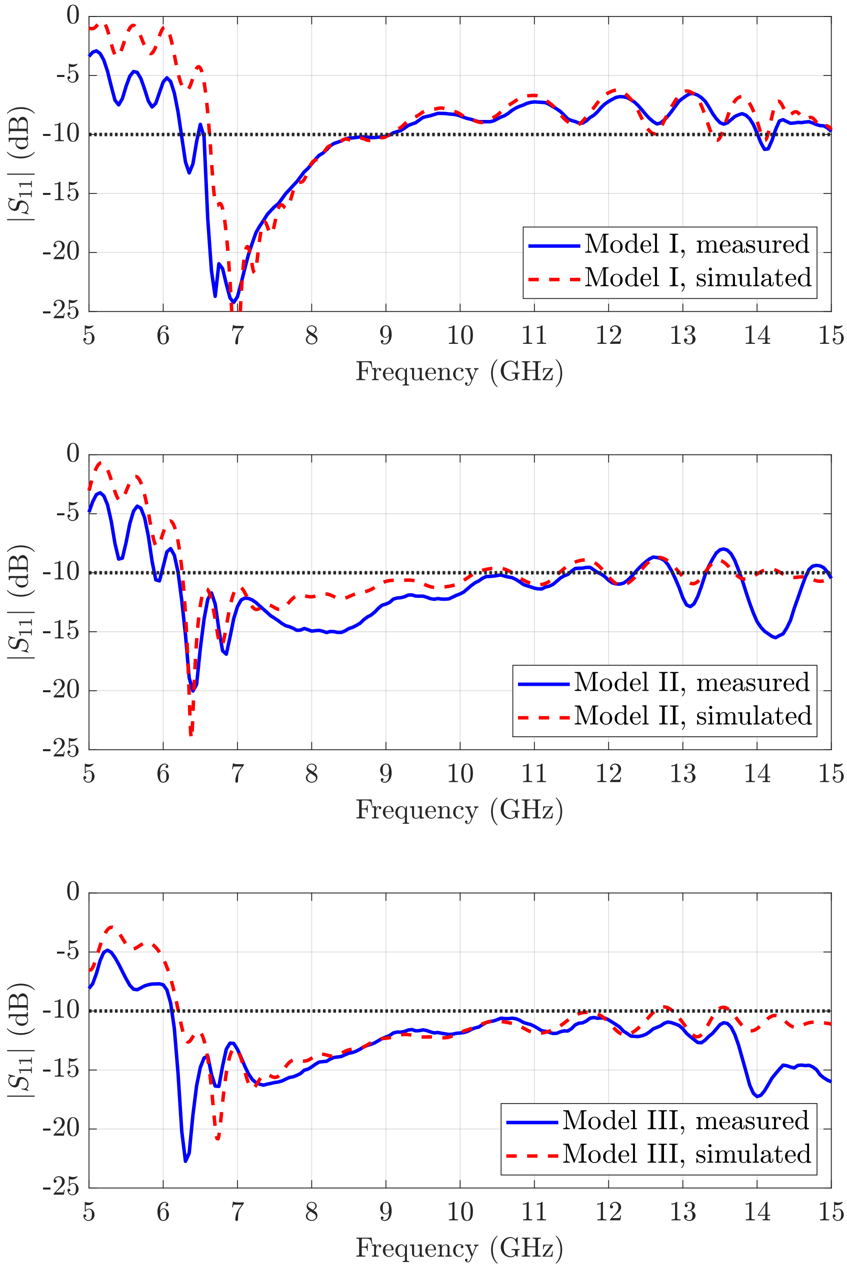

Source: Prepared by the author, 2024

Fig. 15 shows the axial ratio (AR) in decibel as a function of frequency, and once again, we observe a strong agreement between the measurement and simulation results. All the evaluated antennas exhibit AR values less than 3 dB across the entire X band. The standard cylindrical helical antenna, Model I, has the least favorable response. The enhancement in AR response is evident with the non-uniform coil spacing used in antennas

Models II and III. Similar conclusions were drawn in (CHEN et al., 2007b) through the analysis of cylindrical helical antennas with coils spaced exponentially apart. Also, it is clear that the non-uniform wire radius of Model III further improves the AR response.

Table 3 provides a comparative analysis between helical-based antennas recently reported in the literature, constructed using 3D printing processes, and the antenna Model III presented in this study. The comparison focuses on several aspects, including the number of turns (N), the impedance bandwidth (IBW) defined by $|S_{11}| < -10$ dB, the peak realized gain in the co-polarization, and the axial ratio less than 3 dB (AR-3 dB) and less than 1 dB (AR-1 dB).

The antenna described in (GHASSEMIPARVIN; GHALICHECHIAN, 2020) was fabricated using a 3D dielectric printing process, followed by nickel and copper metallization. Conversely, the antenna discussed in (WANG et al., 2020) was produced using 3D printing of a dielectric material (zirconia ceramic) without any metallization. The results from the antenna in (PANUSCH et al., 2022), which employed stereolithography (SLA) and selective laser sintering (SLS) technologies, were also included in the comparisons.

The proposed antenna with tapered wire demonstrates superior performance in terms of axial ratio compared to other designs.

Table 3. Performance comparison of 3D-printed helical antennas.

Ref.	N (turns)	IBW (GHz)	Peak gain (dBic)	AR-3 dB (GHz)	AR-1 dB (GHz)
(WANG et al., 2020)	2	4.75–9.5	10	5.59–6.49	5.80–6.01
(PANUSCH et al., 2022), SLS	10	8.16–10.04	6.1	8.3–12*	11.2–11.3
(PANUSCH et al., 2022), SLA	10	8.33–12.13	7.5	8.45–12*	9.7–9.8
This work	8	6.12–15*	10.8	8*–12*	8*–12*

*The asterisk indicates that the measuring range has reached its limit, but the parameter under investigation still meets the given criteria.

Source: Prepared by the author, 2024

Figure 12. Radiation patterns (RHCP and LHCP) for antenna Model I on the principal planes ($\phi = 0°$ and $\phi = 90°$). The solid lines represent the measurement results, while the dashed lines represent the simulation results. (a) Plane $\phi = 0°$ at 8 GHz; (b) Plane $\phi = 90°$ at 8 GHz; (c) Plane $\phi = 0°$ at 10 GHz; (d) Plane $\phi = 90°$ at 10 GHz; (e) Plane $\phi = 0°$ at 12 GHz; (f) Plane $\phi = 90°$ at 12 GHz.

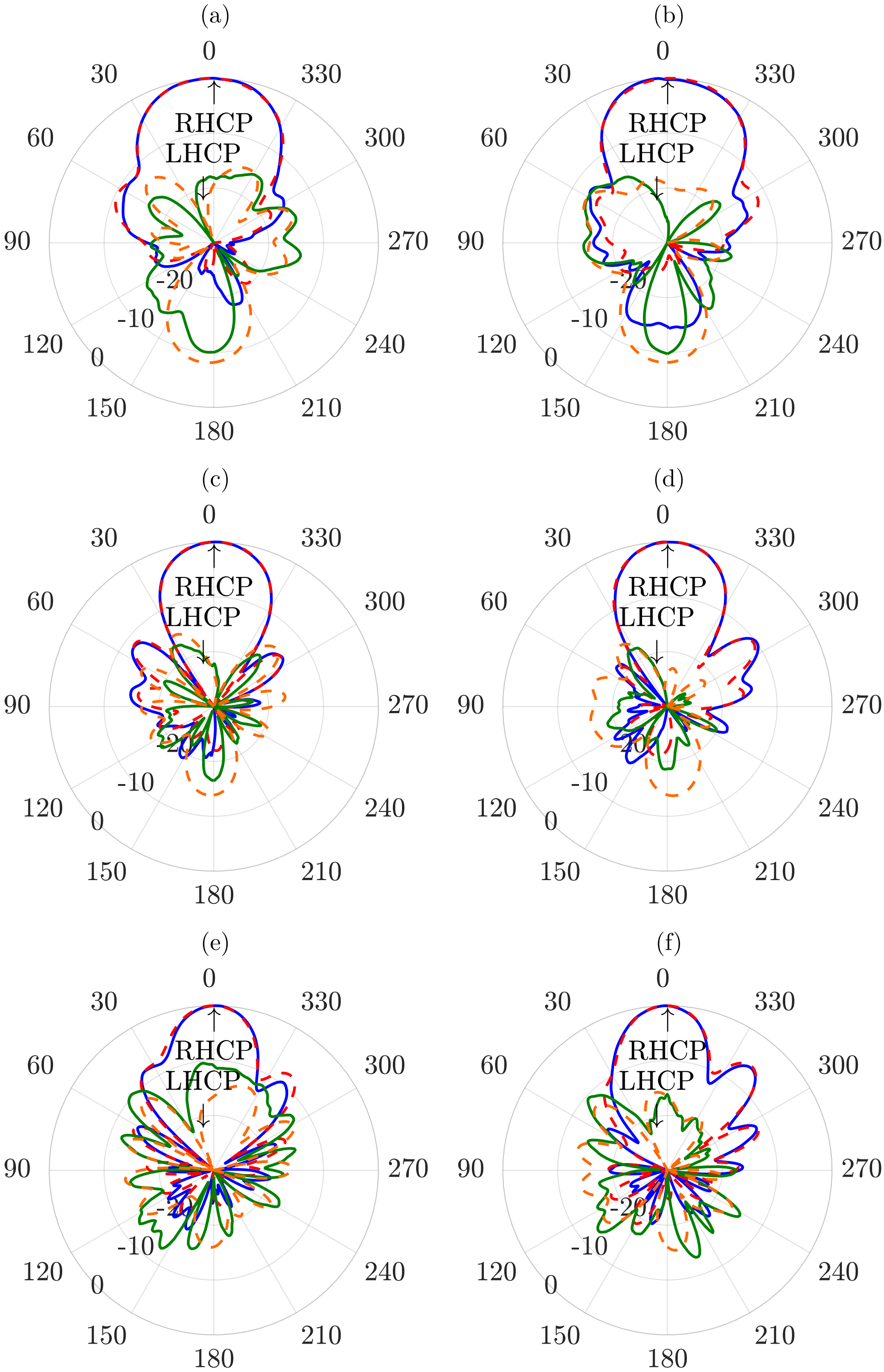

Source: Prepared by the author, 2024

Figure 13. Radiation patterns (RHCP and LHCP) for antenna Model II on the principal planes ($\phi = 0°$ and $\phi = 90°$). The solid lines represent the measurement results, while the dashed lines represent the simulation results. (a) Plane $\phi = 0°$ at 8 GHz; (b) Plane $\phi = 90°$ at 8 GHz; (c) Plane $\phi = 0°$ at 10 GHz; (d) Plane $\phi = 90°$ at 10 GHz; (e) Plane $\phi = 0°$ at 12 GHz; (f) Plane $\phi = 90°$ at 12 GHz.

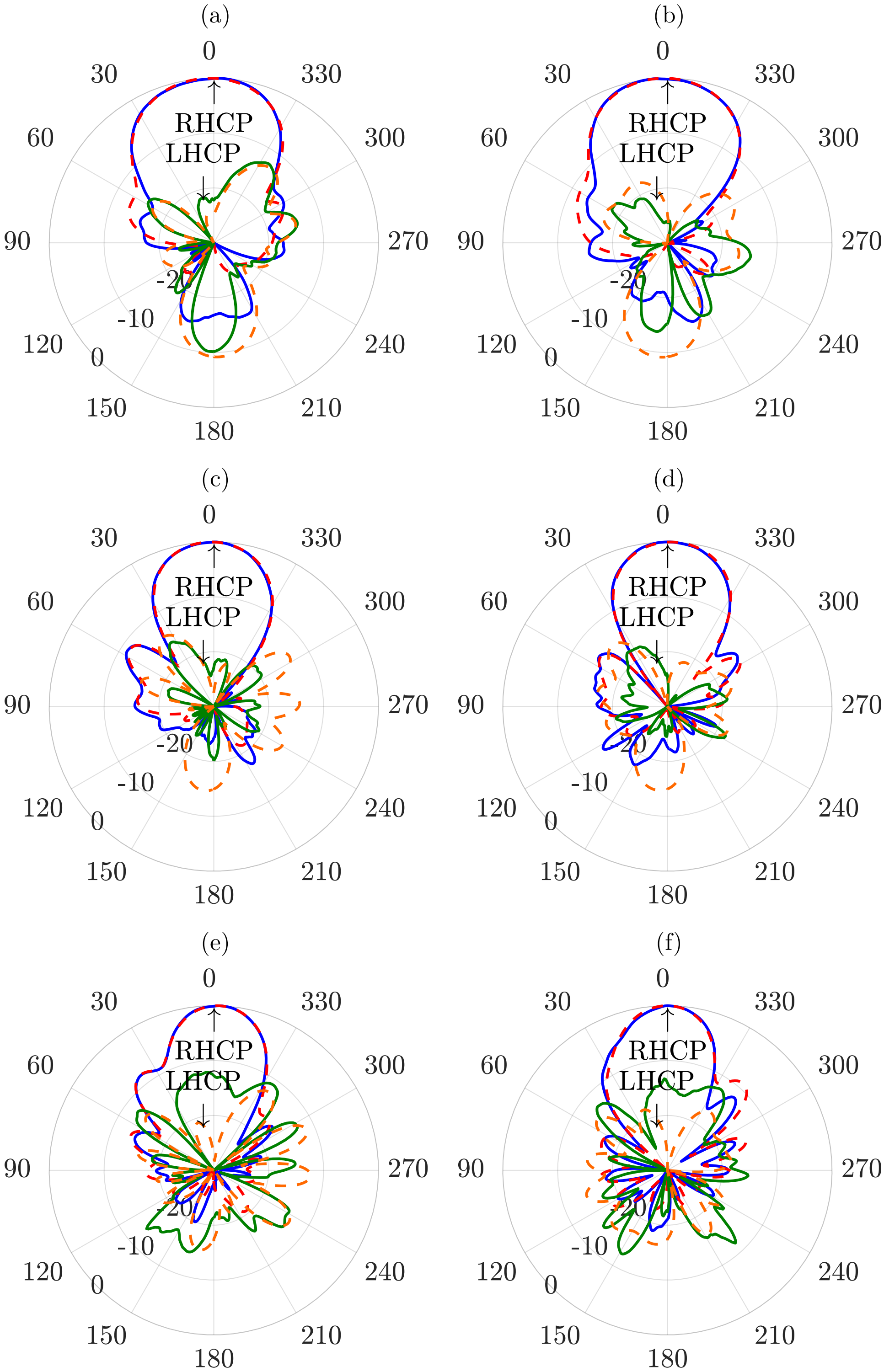

Source: Prepared by the author, 2024

3.3 Advantages of Non-Uniform Wire Cross-Sections

In this section, we delve into the reasons why Antenna Model III outperforms other configurations utilizing uniform-cross-section wires. Given that Antenna Model I exhibits less favorable impedance and axial ratio (AR) bandwidths, the comparisons presented in this section are based on the helix of Antenna Model III (as previously defined, with non-uniform wire radii $r_L = 1.5$ mm and $r_N = 0.5$ mm) and its variations regarding the wire cross-section: Model III-A and Model III-B. The former features a uniform wire cross-section of $r_L = r_N = 0.5$ mm, while the latter has $r_L = r_N = 1.5$ mm. Additionally, since Antenna Model II features an intermediate uniform wire with $r_L = r_N = 1$ mm, it will be included in the comparisons presented in this section.

Fig. 17 presents a comparison of the reflection coefficient of the investigated antennas. The utilization of uniform thick wire (Model III-B) leads to a decrease in the parameter $|S_{11}|$, while the use of thin wire (Model III-A) deteriorates the impedance matching of the antenna. Antenna Model III, utilizing a non-uniform wire with varying thickness along its length, demonstrates the best impedance matching across the entire X-band. The configuration with uniform wire, Model III-B, also exhibits good impedance matching characteristics but is slightly inferior to Model III.

Regarding the maximum realized gain (toward the zenith direction) in left-handed circular polarization (LHCP), the results shown in Fig. 18 indicate that Antenna Model III has a gain approximately 1 dB lower than Antenna Model II. The utilization of uniform thin wire (Model III-A) results in a gain lower than that of the Model II configuration, except near the upper limit of the X-band at 12 GHz, where it slightly surpasses this configuration. Conversely, in the geometry with uniform thick wire (Model III-B), the wire radius significantly impacts the gain, deteriorating below the Model II configuration and worsening as the frequency increases. Regarding the geometry of Antenna Model III with non-uniform wire, at low frequencies, the achievable gain characteristics in right-handed circular polarization (RHCP) are similar to the case with uniform thin wire radius (Model III-A), but they are not as high at high frequencies. However, the gain of Antenna Model III remains more constant over the frequency compared to the other configurations, varying only by 1.74 dB across the X-band. In contrast, Models II, III-A, and III-B configurations vary by 2.14 dB, 3.19 dB, and 2.23 dB, respectively, over the investigated band.

The simulated cross-polarization rejection rate (CPRR), representing the difference between the RHCP and LHCP gains at the zenith direction, is illustrated in Fig. 19 for the examined antennas. All the antennas exhibit a CPRR better than 7.63 dB at the beginning of the X-band. However, the use of uniform thin wire (Model III-A) is the least favorable option at the outset of the X-band. The results show that Antenna Model III-A outperforms the CPRR of other configurations as the frequency increases up to 12 GHz. The minimum CPRR for the antennas increases as the uniform wires become thicker, with values of 7.63 dB, 9.11 dB, and 8.44 dB for Models III-A, II, and III-B, respectively. Antenna Model III achieves a minimum CPRR of 8.77 dB over the X-band, with the most constant response on this band.

Regarding the axial ratio, from the results in Fig. 20, we observe that the circular polarization deteriorates as the uniform wire radius becomes thicker. Similar conclusions were reached in (DINKIć et al., 2019) when analyzing the impact of uniform helical wire radii. Antenna Model III-A, with a uniform thin wire, outperforms other configurations. The impact of the non-uniform wire in Antenna Model III, however, does not compromise the AR response, as it demonstrates comparable performance to that of Antenna Model III-A.

It is crucial to emphasize that we have observed not only a decrease of approximately 1 dB in the realized gain but also a slight reduction in the directivity of Antenna Model III compared to the others in the right-handed circular polarization (RHCP) within the X-band frequency range. In essence, this suggests that the radiation efficiency of the three antenna models is quite similar. Consequently, the variance in antenna gain stems from the tapering of the wire cross-section, which alters the current distribution along the structure, thereby influencing its overall performance. Nonetheless, the enhancements facilitated by the non-uniform helix wire in reducing S_{11}, axial ratio (AR), and cross-polar radiation levels are evident advantages of Antenna Model III. Furthermore, the peak realized gain in RHCP observed across the X-band spectrum of Antenna Model III demonstrates a more uniform distribution compared to other antennas.

Figure 14. Radiation patterns (RHCP and LHCP) for antenna Model III on the principal planes ($\phi = 0°$ and $\phi = 90°$). The solid lines represent the measurement results, while the dashed lines represent the simulation results. (a) Plane $\phi = 0°$ at 8 GHz; (b) Plane $\phi = 90°$ at 8 GHz; (c) Plane $\phi = 0°$ at 10 GHz; (d) Plane $\phi = 90°$ at 10 GHz; (e) Plane $\phi = 0°$ at 12 GHz; (f) Plane $\phi = 90°$ at 12 GHz.

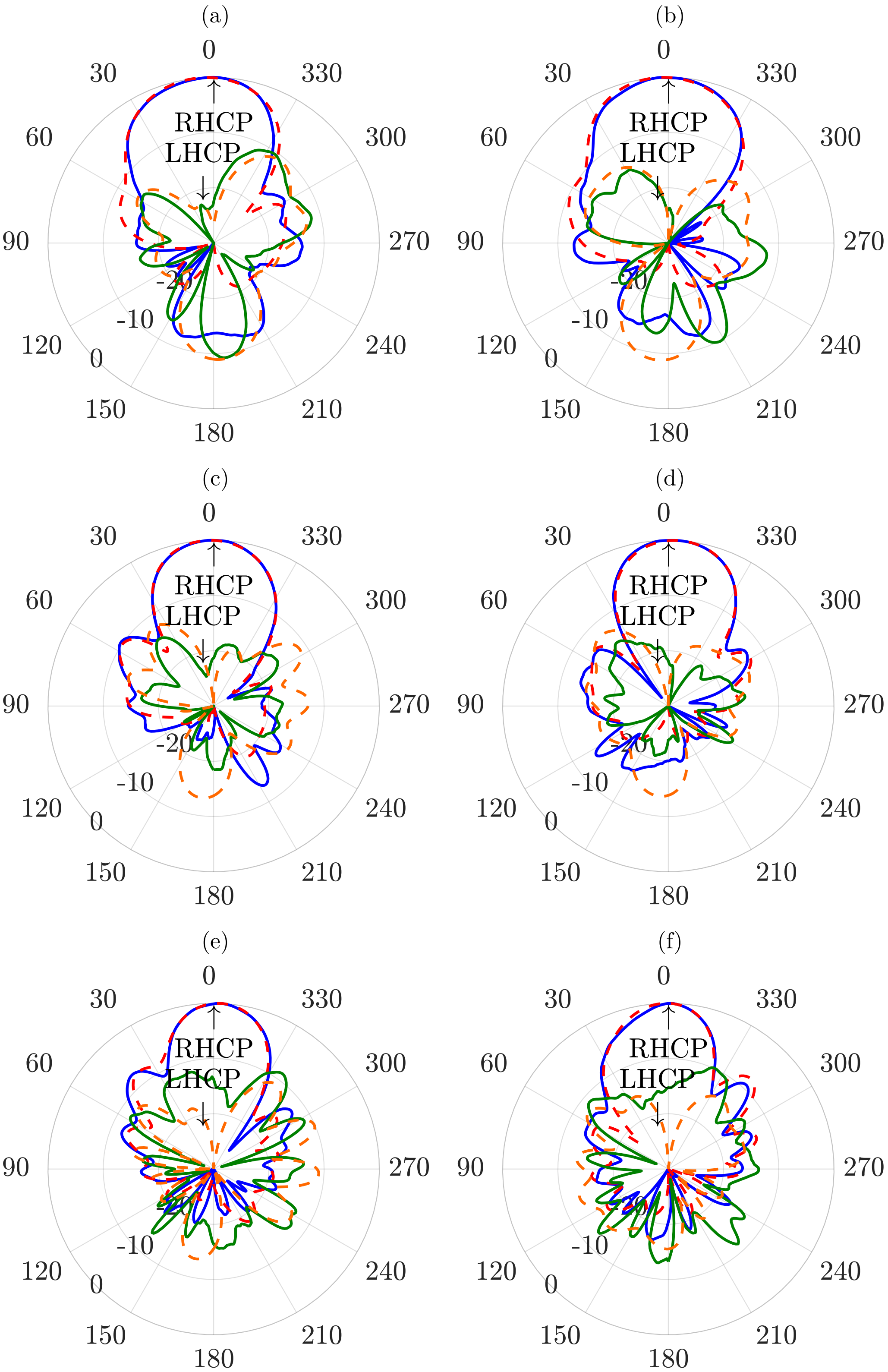

Source: Prepared by the author, 2024

Figure 15. Axial ratio in decibel as a function of frequency. The measurement results are represented by lines, while the simulation results are represented by small symbols.

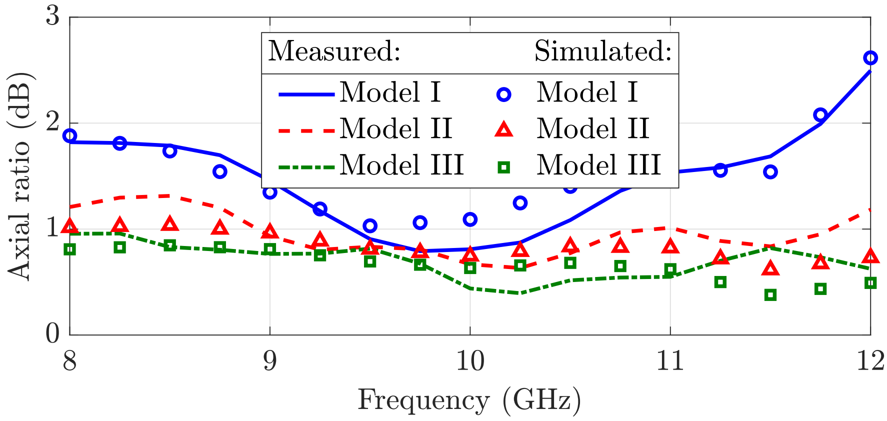

Source: Prepared by the author, 2024

Figure 16. Maximum RHCP realized gain measured for manufactured helical antennas.

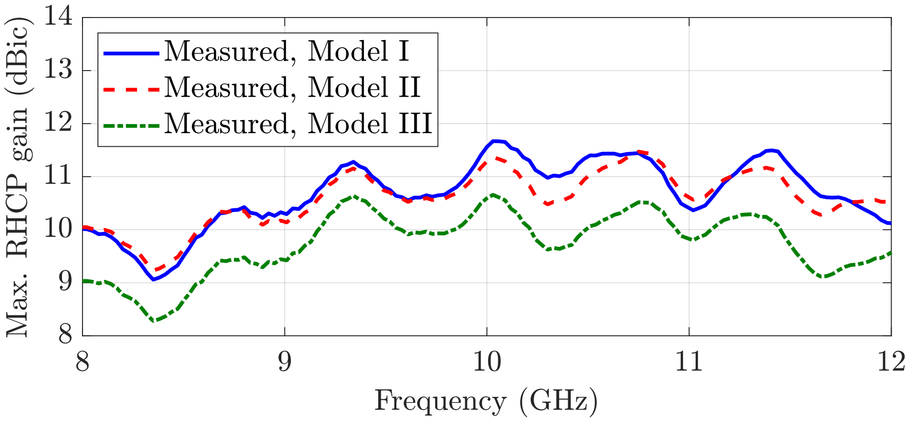

Source: Prepared by the author, 2024

Figure 17. Simulated reflection coefficient as a function of frequency. The reference level, indicated by dotted lines, corresponds to $|S_{11}| = -10$ dB.

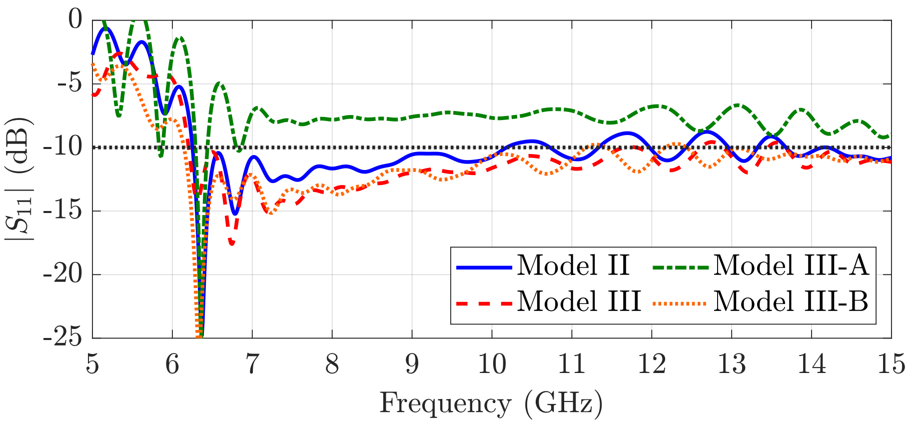

Source: Prepared by the author, 2024

Figure 18. Simulated maximum RHCP realized gain as a function of frequency.

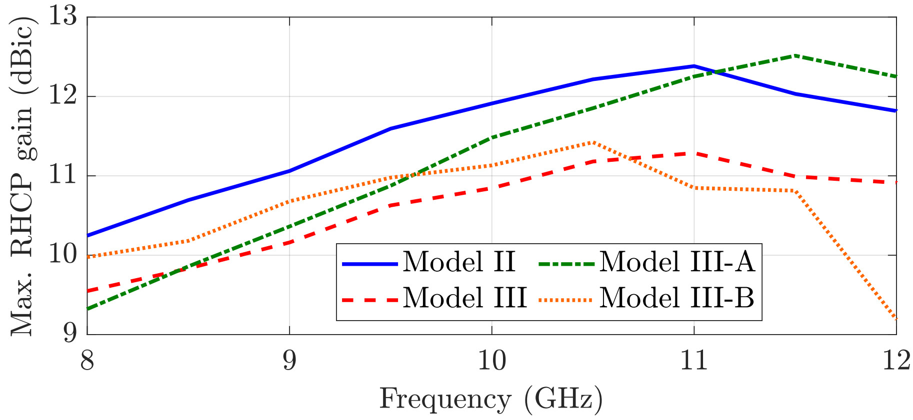

Source: Prepared by the author, 2024

Figure 19. Simulated cross-polarization rejection rate in decibel as a function of frequency.

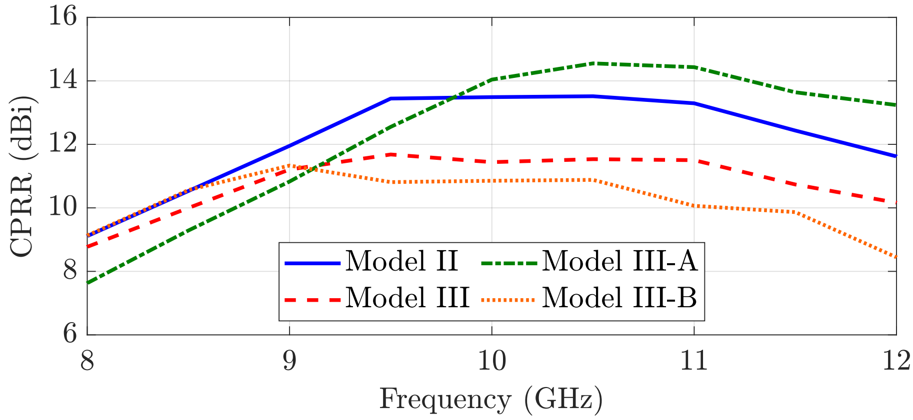

Source: Prepared by the author, 2024

Figure 20. Simulated axial ratio in decibel as a function of frequency

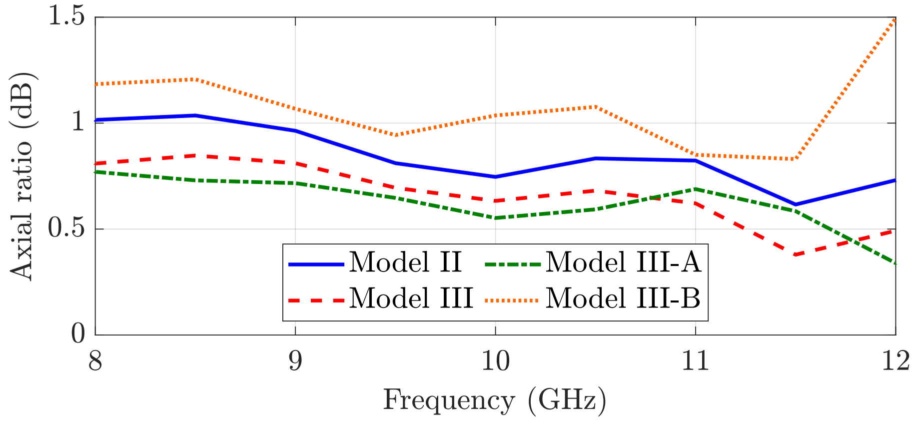

Source: Prepared by the author, 2024

4 Conclusion

Through the integration of additive manufacturing with innovative antenna geometries, a sophisticated product with enhanced electromagnetic performance has been successfully fabricated. Notably, the complexity of these geometries, including variations in diameters and helix spacing, poses significant challenges to manufacturing such products using alternative processes.

The findings unveiled the superior performance of the helical antenna with a tapered cross-section wire compared to the control models. Antenna Model III demonstrates commendable performance across the X-band spectrum, with a measured $|S_{11}| \leq -10$ dB, AR < 1 dB, and peak realized gain in RHCP of 10.8 dBic (with a variation less than 2.4 dB).

It has been observed that utilizing uniform thin wires facilitates favorable radiation characteristics in terms of achievable gain in co-polarization and cross-polarization rejection. However, the impedance matching of these antennas is compromised.

In contrast, antennas using uniform thick wires provide satisfactory impedance matching but demonstrate less favorable radiation characteristics.

The new antenna configuration introduced in this study, which incorporates a non-uniform wire with a thicker base and a thinner tip on the helix, combines the impedance matching of antennas using uniform thick wires with the radiation characteristics of antennas using uniform thin wires. These findings highlight the potential of tapered cross-section wires to improve the performance of helical antennas, offering an additional avenue for optimization in metal additive manufacturing of these antennas.

The non-uniform wire cross-section of Antenna Model III involves a reduction of approximately 1 dB in RHCP gain to enhance various other antenna performance metrics. Further investigation is warranted to explore alternative non-uniform wire helical geometries that do not compromise peak gain.

Bibliography

ABULGASEM, S.; TUBBAL, F.; RAAD, R.; THEOHARIS, P. I.; LU, S.; IRANMANESH, S. Antenna designs for cubesats: A review. *IEEE Access*, v. 9, p. 45289–45324, 2021. Cited on page 18.

ANSYS, Inc. *ANSYS Electronics Desktop 2023*. Canonsburg, Pennsylvania, United States: [s.n.], 2023. 3D High Frequency Simulation Software. Available from Internet: <https://www.ansys.com/products/electronics/ansys-hfss>. Cited 3 times on the pages30, 34, and 39.

AVELINO, A. F.; ARAúJO, W. S.; DIAS, D. F.; dos Santos, L. P. M.; CORREIA, A. N.; de Lima-Neto, P. Corrosion investigation of the 18ni 300 grade maraging steel in aqueous chloride medium containing h2s and co2. *Electrochimica Acta*, v. 286, p. 339–349, 2018. ISSN 0013-4686. Cited on page 24.

BABU, S. S.; LOVE, L.; DEHOFF, R.; PETER, W.; WATKINS, T.; PANNALA, S. Additive manufacturing of materials: Opportunities and challenges. *MRS Bulletin*, Cambridge University Press, v. 40, n. 12, p. 1154–1161, Dec. 2015. Cited 2 times on the pages19 and 22.

BALANIS, C. *Advanced Engineering Electromagnetics*. [S.l.]: Wiley, 2012. (CourseSmart Series). ISBN 9780470589489. Cited on page 19.

BALANIS, C. *Antenna Theory: Analysis and Design*. [S.l.]: Wiley, 2016. ISBN 9781118642061. Cited on page 19.

BALANIS, C. A. *Modern Antenna Handbook*. [S.l.]: Wiley-Interscience, 2008. ISBN 0470036346. Cited 2 times on the pages27 and 34.

BALANIS, C. A. *Antenna Theory: Analysis and Design*. Fourth. Hoboken, NJ: Wiley, 2016. Cited 3 times on the pages17, 18, and 39.

BENECK, R. J.; MACKERTICH-SENGERDY, G.; SOLTANI, S.; CAMPBELL, S. D.; WERNER, D. H. A shape generation method for 3d printed antennas with unintuitive geometries. *IEEE Access*, v. 10, p. 91294–91305, 2022. Cited on page 23.

BYERS, K. J.; BARR, C. Metal additive manufactured freeform antenna. *IEEE Antennas and Wireless Propagation Letters*, v. 17, n. 11, p. 2104–2108, Nov 2018. ISSN 1548-5757. Cited on page 22.

BYUN, G.; CHOO, H.; KIM, S. Design of a dual-band quadrifilar helix antenna using stepped-width arms. *IEEE Transactions on Antennas and Propagation*, v. 63, n. 4, p. 1858–1862, 2015. Cited on page 22.

CHATTERJEE, J. S. Radiation field of a conical helix. *Journal of Applied Physics*, v. 24, n. 5, p. 550–559, 1953. Cited 2 times on the pages22 and 28.

CHE, J.-K.; CHEN, C.-C.; JOHNSON, J. T.; KRAUS, E.; LACZKOWSKI, D.; SOLLY, M. A.; HORGAN, K. 6 GHz to 40 GHz cubesat radiometer antenna system. *IEEE Trans. Antennas Propag.*, v. 67, n. 5, p. 3410–3415, 2019. Cited on page 18.

CHEN, C.-H.; YUNG, E.; HU, B.-J.; XIE, S.-L. Axial mode helix antenna with exponential spacing. *Microwave and Optical Technology Letters*, v. 49, n. 7, p. 1525–1530, July 2007. Cited on page 20.

CHEN, C.-H.; YUNG, E.; HU, B.-J.; XIE, S.-L. Axial mode helix antenna with exponential spacing. *Microw. Opt. Technol. Lett.*, v. 49, p. 1525–1530, 2007. Cited 2 times on the pages22 and 42.

CHEN, Z.; HU, Z.; ZHANG, J.; ZHANG, G.; GUO, C. Compact normal-mode hybrid-helix antenna and its application to circularly polarized yagi array. *IEEE Trans. Antennas Propag.*, v. 69, n. 9, p. 5986–5991, 2021. Cited on page 23.

CUI, L.; ZHANG, Y.; ZHANG, R.; LIU, Q. H. A modified efficient knn method for antenna optimization and design. *IEEE Transactions on Antennas and Propagation*, v. 68, n. 10, p. 6858–6866, 2020. Cited on page 23.

DINKIć, J.; OLćAN, D.; DJORDJEVIć, A.; ZAJIć, A. Design and optimization of nonuniform helical antennas with linearly varying geometrical parameters. *IEEE Access*, v. 7, p. 136855–136866, 2019. Cited 2 times on the pages22 and 46.

DJORDJEVIC, A. R.; ZAJIC, A. G.; ILIC, M. M. Enhancing the gain of helical antennas by shaping the ground conductor. *IEEE Antennas and Wireless Propagation Letters*, v. 5, p. 138–140, 2006. ISSN 1548-5757. Cited on page 20.

DOBBINS, J.; ROGERS, R. Folded conical helix antenna. *IEEE Transactions on Antennas and Propagation*, v. 49, n. 12, p. 1777–1781, 2001. Cited 2 times on the pages22 and 28.

DORLé, A.; GILLARD, R.; MENARGUES, E.; VORST, M. V. D.; RIJK, E. D.; MARTíN-IGLESIAS, P.; GARCíA-VIGUERAS, M. Additive manufacturing of modulated triple-ridge leaky-wave antenna. *IEEE Antennas and Wireless Propagation Letters*, v. 17, n. 11, p. 2123–2127, Nov 2018. ISSN 1548-5757. Cited on page 22.

DYSON, J. The characteristics and design of the conical log-spiral antenna. *IEEE Transactions on Antennas and Propagation*, v. 13, n. 4, p. 488–499, 1965. Cited on page 22.

ERNEST, A. J.; TAWK, Y.; COSTANTINE, J.; CHRISTODOULOU, C. G. A bottom fed deployable conical log spiral antenna design for cubesat. *IEEE Transactions on Antennas and Propagation*, v. 63, n. 1, p. 41–47, 2015. Cited 2 times on the pages18 and 28.

FAERBER, J.; CUMMINS, G.; PAVULURI, S. K.; RECORD, P.; RODRIGUEZ, A. R. A.; LAY, H. S.; MCPHILLIPS, R.; COX, B. F.; CONNOR, C.; GREGSON, R.; CLUTTON, R. E.; KHAN, S. R.; COCHRAN, S.; DESMULLIEZ, M. P. Y. In vivo characterization of a wireless telemetry module for a capsule endoscopy system utilizing a conformal antenna. *IEEE Transactions on Biomedical Circuits and Systems*, v. 12, n. 1, p. 95–105, 2018. Cited on page 18.

FOGED, L. J.; GIACOMINI, A.; MORBIDINI, R.; SACCARDI, F.; SCHIROSI, V.; BOUMANS, M.; GERG, B.; MELACHRINOS, D. Investigation of additive manufacturing for broadband choked horns at x/ku band. *IEEE Antennas and Wireless Propagation Letters*, v. 17, n. 11, p. 2003–2007, Nov 2018. ISSN 1548-5757. Cited on page 22.

GARCíA-MARíN, E.; MASA-CAMPOS, J. L.; SáNCHEZ-OLIVARES, P.; RUIZ-CRUZ, J. A. Evaluation of additive manufacturing techniques applied to ku-band multilayer corporate waveguide antennas. *IEEE Antennas and Wireless Propagation Letters*, v. 17, n. 11, p. 2114–2118, Nov 2018. ISSN 1548-5757. Cited on page 22.

GHASSEMIPARVIN, B.; GHALICHECHIAN, N. Design, fabrication, and testing of a helical antenna using 3d printing technology. *Microw. Opt. Technol. Lett.*, v. 62, n. 4, p. 1577–1580, 2020. Cited 2 times on the pages23 and 42.

HOSSEINI, M.; HAKKAK, M.; REZAEI, P. Design of a dual-band quadrifilar helix antenna. *IEEE Antennas and Wireless Propagation Letters*, v. 4, p. 39–42, 2005. Cited on page 22.

HU, Z.; HUANG, Y.; CHEN, Z.; AL-SHEIKH, A.; CHENG, L.; LIU, Y. Circularly polarized yagi array with small size and symmetric pattern by using counter-wound helix. *International Journal of RF and Microwave Computer-Aided Engineering*, v. 32, n. 9, p. e23286, 2022. Cited on page 23.

KANG, E.; MIN, W.; CHOO, H.; PARK, J.-E. Design of a very high frequency stretchable inverted conical helical antenna for maritime search and rescue applications. *IET Microwaves, Antennas Propagation*, v. 62, n. 1, p. 284–288, January 2020. Cited on page 20.

KIM, O. S. Rapid prototyping of electrically small spherical wire antennas. *IEEE Transactions on Antennas and Propagation*, v. 62, n. 7, p. 3839–3842, 2014. Cited on page 23.

KING, H.; WONG, J. Characteristics of 1 to 8 wavelength uniform helical antennas. *IEEE Transactions on Antennas and Propagation*, v. 28, n. 2, p. 291–296, March 1980. ISSN 1558-2221. Cited on page 20.

K.Jimisha; Kumar, S. Optimum design of exponentially varying helical antenna with non uniform pitch profile. *Procedia Technology*, v. 6, p. 792–798, 2012. Cited on page 20.

KRAUS, J. The helical antenna. *Proceedings of the IRE*, v. 37, n. 3, p. 263–272, 1949. Cited 3 times on the pages22, 27, and 34.

KRAUS, J. *Antennas*. [S.l.]: McGraw-Hill, 1988. (Electrical engineering series). ISBN 9780071004824. Cited 2 times on the pages17 and 18.

KRAUS, J. D. Helical beam antennas. *Eletronics*, v. 20, p. 109–111, April 1947. Cited 2 times on the pages19 and 20.

KRAUS, J. D. Helical beam antennas for wide-band applications. *Proceedings of the IRE*, v. 36, n. 10, p. 1236–1242, Oct 1948. ISSN 2162-6634. Cited on page 20.

KRAUS, J. D. *Antenas*. [S.l.]: McGraw-Hill, 1950. (Electrical Engineering Series). ISBN 9780070354104. Cited on page 20.

KRAUS, J. D. A 50-ohm input impedance for helical beam antennas. *IEEE Transactions on Antennas and Propagation*, v. 25, n. 6, p. 913–913, November 1977. ISSN 1558-2221. Cited 2 times on the pages19 and 20.

KRAUS, J. D.; Williamson, J. C. Characteristics of helical antennas radiating in the axial mode. *Journal of Applied Physics*, v. 19, p. 87–96, January 1948. Cited 2 times on the pages19 and 20.

LAQUERBE, V.; FRAGNIER, R. Metallic S-band antenna for satellite TT & C links. *IEEE Antennas Wireless Propag. Lett.*, v. 21, n. 4, p. 715–719, 2022. Cited on page 18.

LI, W. T.; TANG, H. S.; CUI, C.; HEI, Y. Q.; SHI, X. W. Efficient online data-driven enhanced-xgboost method for antenna optimization. *IEEE Transactions on Antennas and Propagation*, v. 70, n. 7, p. 4953–4964, 2022. Cited on page 23.

NAKANO, H.; MIKAWA, T.; YAMAUCHI, J. Investigation of a short conical helix antenna. *IEEE Transactions on Antennas and Propagation*, v. 33, n. 10, p. 1157–1160, 1985. Cited 2 times on the pages22 and 28.

NAKANO, H.; SAMADA, Y.; YAMAUCHI, J. Axial mode helical antennas. *IEEE Transactions on Antennas and Propagation*, v. 34, n. 9, p. 1143–1148, Sep. 1986. ISSN 1558-2221. Cited on page 20.

NAKANO, Y. S. H.; YAMAUCHI, J. Axial mode helical antennas. *IEEE Transactions on Antennas and Propagation*, v. 34, n. 9, p. 1143–1148, 1986. Cited 2 times on the pages22 and 27.

PANUSCH, D.; HUBERT, F.; BACHBAUER, F.; LOMAKIN, K.; GOLD, G. Additively manufactured helix antenna for x-band applications. In: *2022 16th European Conference on Antennas and Propagation (EuCAP)*. [S.l.: s.n.], 2022. p. 1–4. Cited 2 times on the pages23 and 42.

PENCHEL, R. A.; MARTINS, N. F.; ALDAYA, I.; de Oliveira, J. A.; dos Santos, M. P.; JARDINI, A. L.; AVILA, J.; ROSA, G. S. Performance evaluation of a novel monofilar helical antenna with tapered cross-section wire fabricated via metal additive manufacturing. *AEU - International Journal of Electronics and Communications*, v. 175, p. 155085, 2024. ISSN 1434-8411. Available from Internet: <https://www.sciencedirect.com/science/article/pii/S1434841123005599>. Cited 2 times on the pages24 and 37.

SANTOS, P. L.; AVILA, J. A.; FONSECA, E. B. da; GABRIEL, A. H.; JARDINI, A. L.; LOPES Éder S. Plane-strain fracture toughness of thin additively manufactured maraging steel samples. *Additive Manufacturing*, v. 49, p. 102509, 1 2022. ISSN 22148604. Available from Internet: <https://linkinghub.elsevier.com/retrieve/pii/S2214860421006564>. Cited 2 times on the pages24 and 37.

SHATROV, A. D.; SIVOV, A.; CHUPRIN, A. Investigation of multifilar helical antennas with small radius and large pitch angle on basis of eigenmodes of infinite sheath helix. *Electronics Letters*, v. 30, n. 15, p. 1558–1560, 1994. Cited on page 22.

STROJNY, B. T.; ROJAS, R. G. Bifilar helix gnss antenna for unmanned aerial vehicle applications. *IEEE Antennas and Wireless Propagation Letters*, v. 13, p. 1164–1167, 2014. Cited 2 times on the pages18 and 22.

TAWK, Y. A dynamic dual tapered 3-d printed nested helical antenna. *IEEE Transactions on Antennas and Propagation*, v. 68, n. 2, p. 697–702, 2020. Cited on page 23.

VOLAKIS, J. *Antenna Engineering Handbook, Fourth Edition*. [S.l.]: Mcgraw-hill, 2007. ISBN 9780071475747. Cited on page 18.

WANG, S.; ZHU, L.; LI, Y.; ZHANG, G.; YANG, J.; WANG, J.; WU, W. Radar cross-section reduction of helical antenna by replacing metal with 3-d printed zirconia ceramic. *IEEE Antennas Wireless Propagation Letter*, v. 19, n. 2, p. 350–354, 2020. Cited on page 42.

WHEELER, H. A. A helical antenna for circular polarization. *Proceedings of the IRE*, v. 35, n. 12, p. 1484–1488, Dec 1947. ISSN 2162-6634. Cited on page 20.

WONG, J.; KING, H. Broadband quasi-taper helical antennas. *IEEE Transactions on Antennas and Propagation*, v. 27, n. 1, p. 72–78, January 1979. ISSN 1558-2221. Cited on page 20.

WU, Q.; WANG, H.; HONG, W. Multistage collaborative machine learning and its application to antenna modeling and optimization. *IEEE Trans. Antennas Propag.*, v. 68, n. 5, p. 3397–3409, 2020. Cited on page 23.

YANG, F.; ZHANG, P.; GUO, C.-J.; XU, J.-D. Axial-mode elliptical helical antenna with variable pitch angle. *Electronics Letters*, v. 44, p. 1103–1104, September 2008. Cited on page 22.

ZHOU, Y.; FANG, S.; LIU, H.; FU, S. A liquid metal conical helical antenna for circular polarization-reconfigurable antenna. *International Journal of Antennas and Propagation*, v. 2016, p. 7 pages, 2016. Cited on page 28.